MODELLING POLYMER-INDUCED ADHESION BETWEEN CHARGED MEMBRANES: THEORETICAL AND COMPUTATIONAL APPROACH

A Thesis
Presented to
The Academic Faculty
by

Pannuzzo Martina

In Partial Fulfillment
Of the Requirements for the Degree
Doctor of Philosophy in Chemical Science

University of Catania
December 2011

INTRODUCTION

Membrane fusion and fission are ubiquitous and fundamental processes in biological systems. Cells use them to transport material both between intracellular compartments and out of cells: this is the typical mechanism, e.g. for hormone secretion and for vesicle mediated synaptic transmission[1,2,3,4.]

Several chemical substances have an influence on the fusion rate. Most of them form tight ligand-receptor pairs between nearby membranes bringing them to contact distance from different membrane-anchored proteins[1,2,3,4] to simple divalent cations[4.]

The addition of water soluble polymers that do not appreciably interact with the vesicles' surfaces can dramatically enhance the adhesion/fusion rate[5]. The most common one is polyethylene glycol (PEG). If these same polymers are grafted to a vesicle's surface they have, counterintuitively, the opposite effect[6]. The role of polymer-soluble polymers in triggering adhesion/fusion process between cells or vesicles has been explained in terms of osmotic forces related to the depletion of bulky polymer coils from the inter-membrane gap[6]. It is also well known that PEG condenses even charged macromolecules such as DNA[7,8] , proteins[9], fibrils[10] and microtubules[11].

The above scenario still remains complex even if we consider the mixing properties among ions, polymer and water alone, leaving aside their interactions with suspended particles like vesicles. The good solubility of ions in polymeric solutions or pure polymer melts is well documented due to its many technological applications[12]. However, it is also well-known that in polar solvents, such as water, ions might prefer the more polar aqueous environment. Studies of polymer-ion interactions in solvents of different polarity have been performed by several authors[13,14.]

When the solvation energy overcomes the polymer-solvent mixing entropy, ions induce a phase separation of the homogeneous solution leading to a polymer-rich phase coexisting with a polymer-poor solution in which most of the ions are dissolved. Such aqueous biphasic systems have been widely investigated due to their applicability as solvents in separation processes (for a recent review see, e.g., refs. 15 and 16) and proteins crystallisation[17,18].

In this thesis, we combine the above concepts, namely polymer related

depletion forces and polymers' tendency to phase separate. The goal is to develop a self-consistent picture in which depletion, electrostatics and solvation forces are taken into account to determine the overall behaviour of membrane-membrane interactions in mixed solvents.

We do not explicitly investigate the outstanding polymer effect on the membrane fusion rate, rather we focus on the preliminary polymer-induced adhesion process which appears to be the clue for the following merging of the membrane leaflets.

The rest of the thesis is organized as follows. In chapter 1 we discuss a semi quantitative theory to describe the adhesion kinetics between soft object via the nucleation and lateral growth of a localized adhesion site. In chapter 2, we develop a mean-field model to investigate the non-ideal mixing properties of polymer-containing electrolyte solutions. This calculation will provide the basis for the next chapter. In chapter 3 we extend the model by considering the interactions between two planar charged membranes in contact with a polymer-containing electrolyte solution. In chapter 4 we describe the computational approach. The main predictions of are summarized and compared with experimental and simulation data in chapter 5. In chapter 6 we extend the computational approach to follow the spontaneous evolution of the modelled system in different cases. In chapter 7 we draw the conclusions.

1. NUCLEATION THEORY WITH DELAYED INTERACTIONS

THE JOURNAL OF CHEMICAL PHYSICS 132, 045103 (2010)

Nucleation theory with delayed interactions: An application to the early stages of the receptor-mediated adhesion/fusion kinetics of lipid vesicles

Antonio Raudino[a] and Martina Pannuzzo
Dipartimento di Scienze Chimiche, Università di Catania, Viale A. Doria, 6-95125 Catania, Italy

(Received 25 March 2009; accepted 2 December 2009; published online 28 January 2010)

A semiquantitative theory aimed to describe the adhesion kinetics between soft objects, such as living cells or vesicles, has been developed. When rigid bodies are considered, the adhesion kinetics is successfully described by the classical Derjaguin, Landau, Verwey, and Overbeek (DLVO) picture, where the energy profile of two approaching bodies is given by a two asymmetrical potential wells separated by a barrier. The transition probability from the long-distance to the short-distance minimum defines the adhesion rate. Conversely, soft bodies might follow a different pathway to reach the short-distance minimum: thermally excited fluctuations give rise to local protrusions connecting the approaching bodies. These transient adhesion sites are stabilized by short-range adhesion forces (e.g., ligand-receptor interactions between membranes brought at contact distance), while they are destabilized both by repulsive forces and by the elastic deformation energy. Above a critical area of the contact site, the adhesion forces prevail: the contact site grows in size until the complete adhesion of the two bodies inside a short-distance minimum is attained. This nucleation mechanism has been developed in the framework of a nonequilibrium Fokker–Planck picture by considering both the adhesive patch growth and dissolution processes. In addition, we also investigated the effect of the ligand-receptor pairing kinetics at the adhesion site in the time course of the patch expansion. The ratio between the ligand-receptor pairing kinetics and the expansion rate of the adhesion site is of paramount relevance in determining the overall nucleation rate. The theory enables one to self-consistently include both thermodynamics (energy barrier height) and dynamic (viscosity) parameters, giving rise in some limiting cases to simple analytical formulas. The model could be employed to rationalize fusion kinetics between vesicles, provided the short-range adhesion transition is the rate-limiting step to the whole adhesion process. Approximate relationships between the experimental fusion rates reported in the literature and parameters such as membrane elastic bending modulus, repulsion strength, temperature, osmotic forces, ligand-receptor binding energy, solvent and membrane viscosities are satisfactory explained by our model. The present results hint a possible role of the initial long-distance → short-distance transition in determining the whole fusion kinetics. © *2010 American Institute of Physics.* [doi:10.1063/1.3290823]

1.1. Schematic picture of the system

Consider two identical large vesicles brought in the initial state at the equilibrium distance D (Fig.1).

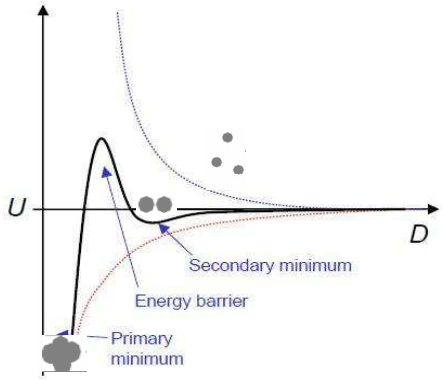

Fig 1 Energy profile vs distance

Typically, the energy-distance curve exhibits two minima: a shallow long-distance minimum (the so-called secondary minimum) at $z = D$ and a deep short-distance well at $z = D - 2\eta_{MAX}$ (the primary minimum). The energy-distance curve arises from different contributions.

The classical DLVO theory[19] **of colloid particles considers a combination of repulsive electrostatic forces and attractive van der Waals interactions**. Their combination may give rise to an energy double well profile. **In biological membranes other contributions must be accounted for.** For instance, the strongly hydrophilic membrane surface induces overwhelming short-range repulsive hydration forces due to water ordering at polar interfaces[20,21]

Besides, long-range repulsion forces arising from the protruding hydrophilic sugar residues of glycolipids and glycoproteins[22] have to be considered. At short distance, the repulsive forces are generally stronger than the dispersion ones. However, specific molecules may form tight ligand-receptor bonds between nearby membranes yielding a sharp minimum at distances comparable with the ligand size[23] (Fig.1). A common biomimetical system is the biotin-streptavidin couple, but also simple divalent cations are effective in bridging negatively charged membranes.

A cartoon of the process is given in Fig.2 where **the evolution from loosely bound (left) to tight bound (right) large vesicles via the formation of a localised dimple** is reported.

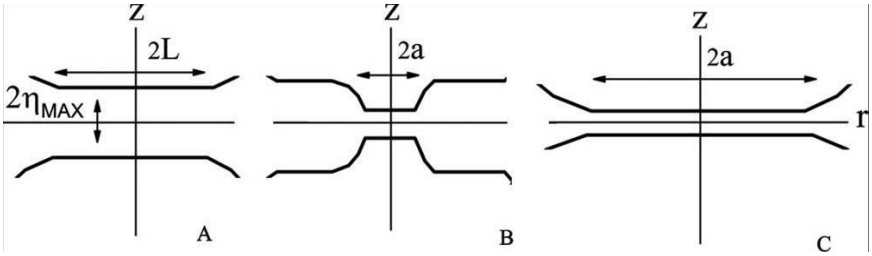

Fig 2 Evolution from loosely bound (left) to tight bound (right) large vesicles (adapted from 31)

For simplicity only the vesicles adhesion region has been drawn. The contact area of strongly (left) and weakly (right) bound states appreciably differs, the size L of the weakly bound state depending on the adhesion energy and vesicle radius[24], in any case L is much greater than the critical adhesion plaque radius a^*.

The mechanism sketched above suggests an alternative route for the long-distance $\rightarrow$ short-distance transition of "soft" particles. **When the particles rigidity is small and/or their size is large, this route is an efficient alternative to the undeformed approach mechanism (DLVO theory) still valid in modelling adhesion/fusion kinetics of very small vesicles**[25]

The picture described so far accounts for early stages of the fusion process that may further evolve through more steps. Let us consider in detail the **whole fusion process among vesicles V :**

$$V + V \Leftrightarrow V_2^{loose} \rightarrow V_2^{tight} \rightarrow \underbrace{T_1 \rightarrow T_2 \rightarrow \ldots T_n \rightarrow \ldots}_{N} \rightarrow P$$

The first reversible step $V + V \Leftrightarrow V_2^{loose}$ is diffusion-controlled, while the second one $V_2^{loose} \rightarrow V_2^{tight}$ is slow and basically irreversible. It may occur either by approaching the undeformed membranes (as in the DLVO theory) or via a dimple formation like in the present model. **The transition to the short-distance minimum is followed by a displacement of the lipid polar headgroups giving rise to hydrophobic patches. They attract each other until the external part of the contacting membrane bilayers merge forming a stalk. Stalk formation and evolution, $V_2^{tight} \rightarrow T_1 \rightarrow T_2 \rightarrow ...T_n \rightarrow \cdots$, can be thought as a cascade of N intermediates describing the merging of the tight adhering membranes into a new bigger vesicle P. The**

structure of the different fusion intermediates (stalk, hemi-fusion, pre-pore and connecting pore) has been postulated and/or observed.

In some cases, the short-distance adhesion might be the bottleneck to the whole fusion process because of the lateral tension developing in strongly adhering vesicles[26]. At tight adhesion, the tension is so strong that membranes destabilization and fracture is likely when they are stretched beyond a critical value[27] (lipid membranes cannot be stretched beyond 2-4% without rupturing[28.] In other cases, vesicles strongly adhere but do not fuse because of the high energy of the stalk. In any case, **the formation of tight adhering membrane patches is a fundamental step in the fusion process**. The well-known fusogenic behaviour of hydrophilic polymers can be understood in term of enhanced adhesion, while it is hard to conjecture that the stalk energy, mainly related to the structure of the membrane inner core, is modified by polymer dissolved in the aqueous phase.

We focus on the initial process $V + V \Leftrightarrow V_2^{loose} \rightarrow V_2^{tight}$.

1.2. Formation energy of an adhesion patch

1.2.1. Bending Energy

Following Helfrich[29] the bending energy of an isolated elastic membrane is $E_{bend} = \int_S \left(\frac{1}{2} K_M (C_1 + C_2 - C_o)^2 + K_G C_1 C_2 \right) dS$, where C_1 and C_2 are the principal curvatures, C_o the spontaneous curvature ($C_o = 0$ for planar membranes), K_M is the bending rigidity per unit area and K_G the elastic modulus of Gaussian curvature. The integration is extended over the whole membrane surface S. The elastic constants K_M and K_G can be obtained from experiments or predicted from the membrane structure. Typically[30] $K_M \approx 10^{-13} - 10^{-12} erg$. Consider two identical membranes, A and B,

undergoing local deformations η_A and η_B, in the Helfrich approximation we re-write the above equation as

$$E_{bend} = \sum_{j=A,B} \iint_{S>S_o} \left[\frac{1}{2} K_M \left(\frac{\partial^2 \eta_j}{\partial x^2} + \frac{\partial^2 \eta_j}{\partial y^2} \right)^2 + K_G \left(\frac{\partial^2 \eta_j}{\partial x^2} \frac{\partial^2 \eta_j}{\partial y^2} - \left(\frac{\partial^2 \eta_j}{\partial x \partial y} \right)^2 \right) \right] dxdy \qquad (1)$$

The integration is extended outside the adhesion site, $S > S_o$, while in the region $S < S_o$ the bending energy is zero because the adhesion plaque is planar.

1.2.2. Interaction energy

The bending energy must be supplemented by the repulsion energy between the membranes. As said before, in the initial state the membrane stays in a shallow long-distance minimum (Fig.2, left panel). On approaching the membranes along their perpendicular $z-$ axis the energy first increases, thereafter it falls inside a short-distance minimum (Fig.1). Adopting a phenomenological picture, we approximate the membrane-membrane interaction outside the plaque ($S > S_o$) by a quadratic function of the deformation: $E_{rep} = \frac{1}{2} F \iint_{S>S_o} (\eta_A - \eta_B)^2 dxdy$. The coefficient F can be derived from experimental measurements or predicted from the membrane structure. Inside the plaque ($S < S_o$) the deformation takes its largest value ($\eta_A(x,y) = -\eta_{MAX}$, $\eta_B(x,y) = +\eta_{MAX}$), then the above formula reduces to $E_{rep} = \frac{1}{2} F (2\eta_{MAX})^2 S_o$. Combining the two terms

$$E_{rep} = \frac{1}{2} F \left(4\eta_{MAX}^2 S_o + \iint_{S>S_o} (\eta_A - \eta_B)^2 dxdy \right) \qquad (2)$$

1.2.3. Bridging energy

Inside the adhesion disk the membrane distance is short enough to allow the formation of *Cis* complexes tightly joining the opposite membranes. The bridging energy is written as

$$E_{bridge} = -E_C \sigma_C \theta_C S_o \qquad (3)$$

where $-E_C$ is the sticking energy per complex, σ_C the two-dimensional stickers concentration, S_o the adhesion plaque area and $0 < \theta_C < 1$ the fraction of stickers that form *Cis* complexes.

Adding together contributions (1)-(3)

$$E_{TOT} = (2F\eta_{MAX}^2 - E_C\sigma_C\theta_C)S_o + \frac{1}{2}K_M \iint_{S>S_o} \left[\left(\frac{\partial^2\eta_A}{\partial x^2} + \frac{\partial^2\eta_A}{\partial y^2} \right)^2 + \left(\frac{\partial^2\eta_B}{\partial x^2} + \frac{\partial^2\eta_B}{\partial y^2} \right)^2 + 2\frac{K_G}{K_M} \left(\frac{\partial^2\eta_A}{\partial x^2}\frac{\partial^2\eta_A}{\partial y^2} - \left(\frac{\partial^2\eta_A}{\partial x \partial y} \right)^2 + \frac{\partial^2\eta_B}{\partial x^2}\frac{\partial^2\eta_B}{\partial y^2} - \left(\frac{\partial^2\eta_B}{\partial x \partial y} \right)^2 \right) + \frac{F}{K_M}(\eta_A - \eta_B)^2 \right] dxdy \qquad (4)$$

After some algebra given in ref.[31] enabling us to express the optimized adhesion energy as a function of the adhesive disk radius a, $E_{xcess}(a) \equiv E_{TOT}(a) - E_{FLAT}$ (defined as the difference between the energy of the patch-forming membranes and that of the flat membranes at equilibrium distance), we find to the leading term:

$$E_{EXCESS} = \frac{1}{2}(A_2 - A_3)a^2 + A_1 a \qquad \mu a >> 1 \qquad (5)$$

where: $A_2 \equiv 4\pi F\eta_{MAX}^2$; $A_3 \equiv 2\pi E\sigma_C\theta_C$; $A_1 \equiv \pi 2^{7/4}\eta_{MAX}^2 F^{3/4}K_M^{1/4}$; $B \equiv 2^{7/2}\eta_{MAX}^2 F^{1/2}K_M^{1/2}$.

For that concerns biological membranes, when $\mu a >> 1$, the membranes pay a huge energy cost to form an adhesion site. On the contrary, the less common case describes either slightly repelling membranes or extremely tight ligand-receptor bridges, where we may suppose the adhesion site to be pointlike.

It is worth discussing the energy behaviour. The first term of eq.(5), $\frac{1}{2}(A_2 - A_3)a^2$, accounts for the balance between adhesion and repulsion forces inside the adhesion disk, while $A_1 a$ describes the energy outside the disk. The linear dependence

on a means that the elastic energy is located in a narrow strip around the disk periphery. When $A_2 - A_3 > 0$ (repulsive energy greater than adhesion), the energy monotonously grows with a, but when $A_2 - A_3 < 0$ (repulsive energy smaller than adhesion) the energy first reaches a maximum, then decreases (fig.3). In this nucleation process only nuclei bigger than a critical size further grow until full membrane adhesion is attained. The non-equilibrium concentration of the critical nuclei is calculated in the forthcoming section.

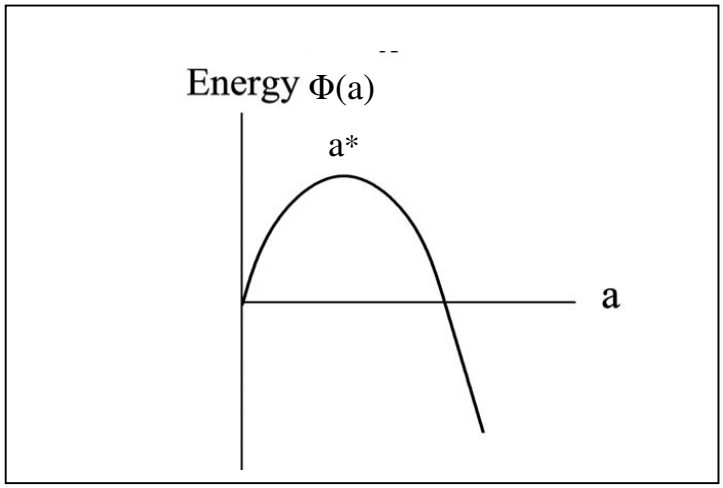

Fig. 3 Energy profile when $A_2 - A_3 < 0$ (repulsive energy smaller than adhesion).

1.3. Nucleation rate

Sudden ligand-receptor bridging (x→∞)

According to the classical non-equilibrium theory of nucleation processes, **the time evolution of the nuclei distribution** $P(a,t)$ **in the space of nuclei size** a satisfies the continuity equation[32]

$$\frac{\partial P}{\partial t} = -\frac{\partial J}{\partial a} \qquad (6)$$

where $J \equiv J(a,t)$ is the flux of nuclei going from the size a to $a+da$.

The flux arises from competing condensation and dissolution processes, acontinuum picture yields

$$J(a,t) = -D_{\|}(a) P_{eq} \frac{\partial}{\partial a}(P / P_{eq}) \qquad (7)$$

where the equilibrium distribution is: $P_{eq}(a) = P_o \exp\left(-\Phi(a)/kT\right)$. P_o defines the concentration of the smallest nuclei (embryos) and $\Phi(a)$ is the minimal work needed to form a nucleus of radius a. We may identify $\Phi(a) = E_{EXCESS}$, this latter being the energy of two nearby membranes connected through an adhesion patch given by eq.(5). $D_{\|}(a)$ plays the role of a "diffusion coefficient" in the space of nuclei sizes.

A compact expression for the steady rate of nuclei production is:

$$J_S \approx \frac{2}{\sqrt{\pi}} P_o D_{\|}(a^*) \left(-\frac{1}{kT} \frac{\partial^2 \Phi}{\partial a^2}\bigg|_{a=a^*} \right)^{1/2} \exp\left(\frac{\Phi(a^*)}{kT} \right) \qquad (8)$$

The model developed so far describes most nucleation processes like the formation of a solid from a fluid phase. Nevertheless, the adhesion/fusion process requires specific models to calculate:

a) The activation barrier to membrane adhesion $\Phi(a)$ which depends on the balance between adhesion forces, compression energy and bending energy.

b) The "diffusion coefficient", $D_{\|}(a)$, a measure of the adhesion plaque growth rate, is related to the membrane fluctuations near the plaque rim. It depends on viscous and elastic forces as well.

c) The probability P_o to form the smallest embryos ($a \to 0$) which is all but nothing the collision probability between nearby fluctuating membranes.

Noninstantaneous bridging kinetics ($\chi \to 0$)

In the other relevant limit $\chi \to 0$ (extremely slow bridging kinetics) the number of bridges remains very small during the plaque growth preventing the formation of stable adhesion sites, thus $\lim_{\chi \to 0} J_S \approx 0$ (9)

1.4. Results and discussion

By hypothesizing that the short-distance adhesion is the bottleneck to the whole fusion process, one may apply the model to rationalize real fusion events.

a) When large vesicles are considered, the model valid for deformable bodies predicts that the barrier to adhesion is independent of vesicle radius R. This result is in sharp contrast with the adhesion models of *rigid* spheres where the rate exponentially decreases with radius[19] Therefore, cell-sized objects would never fuse together because R is too large.

b) According to our model for adhesion to occur a *critical ligand concentration* must be attained. Afterwards, the adhesion rate remains sensitive to the concentration c^- of divalent cations bridging two negatively charged lipids. The following equation:

$$rate \approx \begin{cases} 0 & \bar{c} < c_{crit} \\ \exp\left(-\dfrac{|C_1|}{\bar{c}\,Ee^{+E/kT} - |C_2|}\right) & \bar{c} > c_{crit} \quad small \ \bar{c} \\ \exp\left(-\dfrac{|C_1|}{E - |C'_2|}\right) & \bar{c} > c_{crit} \quad high \ \bar{c} \end{cases} \qquad (10)$$

evidencing a burst of the adhesion rate above a critical ion concentration.

c) The model highlights a strong sensitivity of the fusion rate on the bridging energy E and therefore a great ion specificity (at variance of DLVO theories). Experimentally, the ion specificity has been well established long time ago[33] . It is worth mentioning the dramatic difference between Ca^{2+} and Mg^{2+}, calcium being much more effective in triggering and enhancing the fusion rate.

d) The adhesion rate sharply decreases with the membrane repulsion F roughly as: $rate \approx \exp\left(-|const|\dfrac{F^{3/2}}{1-|C|F}\right)$.

High F are likely in charged membranes, but also neutral phosphatidylcholine (PC) vesicles, the most abundant component of living cells membrane, exhibit large F because of the overwhelming hydration forces[20,21,34,35,36]. This fact explains way PC vesicles do not spontaneously fuse, unless we consider strongly strained small unilamellar vesicles[37] or vesicles squeezed together by depletion forces[38].

e) For planar membranes approaching along their perpendicular axis, the long-distance $\rightarrow$ short-distance transition probability *increases* with the bending rigidity K_M. This is due to the lowering of the undulation forces[39] great at small K_M ($\approx T^2 / K_M$). Conversely, in our model: $rate \approx \exp\left(-|const| K_M^{1/2}\right)$, showing a decrease of the adhesion with K_M. The effect, however, is weaker than that found by increasing the repulsion F. Experimentally, the fusion rate is faster when the membrane is in the fluid phase (low bending rigidity) than in the gel phase where the bending rigidity is up to an order of magnitude higher[40].

f) A pressure $\Im$ applied to the adhering membranes (e.g., osmotic forces induced by water soluble polymers sterically excluded from the inter-vesicles space, usually named as depletion forces) reduces the equilibrium interlamellar distance.

g) The temperature behaviour of the adhesion rate depends both on direct ($rate \approx \exp(-|const|/T)$ and indirect effects, these latter being related to the thermal variation of physical parameters. Among the indirect effects we mention the lowering of membrane rigidity above the thermotropic gel$\rightarrow$fluid phase transition, often accompanied by an increase in the fusion kinetics. Typically, fusion rate increases with T, with a sharp maximum near the membrane transition temperature T°[41]

h) An intriguing result is the behaviour of the fusion rate with solvent viscosity ω. Indeed, the nucleation kinetics depend on the balance between plaque growth v (proportional to $1/\omega$) and dissolution rates. Below a critical size, the dissolution rate

depends on the bridges concentration. In viscous fluids the longer life time of the adhesion enables the formation of more bridges with a consequent lowering of the "dynamic" barrier.

i) Adhesion is faster at high ligand-receptor bridging rate χ. In order to form *Cis* complexes, the charged lipids belonging to opposite membranes must diffuse along the membrane surface and encounter.

The model developed so far does not describe the truly fusion process (the merging of the two contacting membranes with the formation of an expanding pore). This fusion process has been fully investigated by other authors[42] and it will not investigated in our thesis. Notwithstanding, the model addressed in the previous section (the formation of an ion-assisted stable adhesion plaque at contact distance, or, in biochemical language, the "de-hydration" step) probably accounts for the true kinetic transition state of the whole fusion process. This is a consequence the high energy required to form a local protrusion of a lateral critical size.

The overall fusion rate, however, do depend both on the transition state energy barrier, but it is also related to the number of weakly-adhering vesicles pairs contained in the sample. Most of the forthcoming calculations will address this relevant topic. They will describe the well-known polymer effect on the adhesion energy between two identical flat charged membranes set at equilibrium distance. The results will compared with the behaviour of neutral membranes.

2. THERMODYNAMICS OF THE PSEUDO-TERNARY SYSTEM POLYMER+IONS+ SOLVENT

Before to investigate the polymer effect on a pseudo-ternary solution that contains solvent (water), ions and a neutral but soluble polymer. The mixing behavior of this ternary system is not trivial at all. Its properties will for the basis for understanding the polymer effect on the adhesion of charged membranes embedded in a polymer solution.

Let us begin by considering a dilute aqueous electrolyte solution in which a neutral polymer of lower dielectric permittivity is dissolved. We define $c_{\pm}(\mathbf{r})$ to be the local *dimensionless* concentrations of positive and negative single-valent ions, each of them carrying a unit charge $\pm e$, and $c_{Z+}(\mathbf{r})$ as the concentration of multi-valent ions of valence Z_+. In biological systems, $c_{\pm}(\mathbf{r})$ is typically ~10^{-1} M while $c_{Z+}(\mathbf{r})$ (mainly Z=2) is about 10^{-6} M. We require, that the average concentrations ($\bar{c}_i$) of the different ions must satisfy the electroneutrality condition

$$\bar{c}_+ + \bar{c}_{Z+} + \bar{c}_- = 2\bar{c}_M + (Z_+ + 1)\bar{c}_Z \qquad (11)$$

where $\bar{c}_M$ and $\bar{c}_Z$ are the macroscopic concentrations of monovalent and *Z*-valent salts, respectively. We define $\Phi(\mathbf{r})$ to be the local polymer volume fraction, $\bar{\Phi}$ the average polymer volume fraction and N the degree of polymerisation. In the following, we will explore the physically relevant case of semi-dilute polymer solutions defined over the concentration range $N^{-4/5} << \bar{\Phi} << 1$[43]. In this range, the polymer coils overlap but the polymer fraction is still low. This is a situation that allows for a continuum treatment of polymer solutions. At lower concentrations (dilute regime), coils behave like an ideal gas of isolated spheres of the radius $R_G (\approx N^{3/5})$. The energy of the polymer solution is the sum of contributions coming from polymer and electrolytes. We describe these contributions next.

a) Polymer contribution

In a mean-field picture the free energy of a polymer solution can be written as[44,45]

$$E_{POL} = \frac{kT}{a^3}\int_V \left[\frac{a^2}{24\Phi(\mathbf{r})(1-\Phi(\mathbf{r}))}\left(\nabla\Phi(\mathbf{r})\right)^2 + \frac{\Phi(\mathbf{r})}{N}\log\frac{\Phi(\mathbf{r})}{N} + (1-\Phi(\mathbf{r}))\log(1-\Phi(\mathbf{r})) + \chi\Phi(\mathbf{r})(1-\Phi(\mathbf{r})) \right] dV \qquad (12)$$

where k is the Boltzmann constant and T the absolute temperature. a denotes the diameter of a single molecular unit (monomer, ion and solvent) that, for the sake of compactness, are assumed having the same size.

The first term accounts for the energy loss associated to spatial heterogeneities. In polymer solutions, perturbations due to chain-interface boundaries propagate deep inside the fluid. This is at variance with molecular fluids consisting of small molecules where the concentration gradients are localised near the interface. The remaining two terms in (12) describe the homogeneous component of the polymer energy in the Flory-Huggins approximation[43]. The second and third terms describe the polymer and the solvent mixing entropies. Strictly speaking, the solvent contains both solvent molecules and different kinds of ions (monovalent anions and cations and a small amount of Z-valent cations), but in semi-dilute solution we may safely assume: $\Phi_s(\mathbf{r}) = 1-\Phi(\mathbf{r}) - \sum_i c_i(\mathbf{r}) \approx 1-\Phi(\mathbf{r})$. The fourth and final term accounts for the polymer-polymer, polymer-solvent and solvent-solvent interactions as described by the mean-field Flory interaction parameter $\chi = \chi(T)$. The contributions arising from polymer-ion and solvent-ion interactions is added in the following section b.

b) Electrolyte contribution

The good solubility of ions in a melt of hydrophilic polymers is well-known[46.] This property constitutes the basis of several technological applications such as electrolytic fuel cells**Errore. L'origine riferimento non è stata trovata.**. On the other hand, in polar solvents, e.g. water, ions prefer more polar environment[47.] When the solvent

polarization energy overcomes the entropy of mixing (low in polymer solutions because of chain connectivity), ions induce phase separation of homogeneous water/polymer mixtures and the formation of fluid phases.

In order to describe the contribution of the electrolyte in the ternary polymer + solvent + electrolyte system, we decompose the energy of the ions into a sum of two main terms:

i) A standard entropic contribution that for dilute electrolyte solutions takes the simple form:

$$-TS_{ION} = \frac{kT}{a^3}\int_V (c_+(\mathbf{r})(\log c_+(\mathbf{r})-1)+c_-(\mathbf{r})(\log c_-(\mathbf{r})-1)+c_{Z+}(\mathbf{r})(\log c_{Z+}(\mathbf{r})-1))dV$$

ii) The ion-solvent interaction contribution. In homogeneous fluids, the ion-solvent energy of an interaction can be calculated as a function of the fluid dielectric permittivity $\bar{\varepsilon} \equiv \varepsilon(\bar{\Phi})$ and the electrolyte concentration $\bar{c}$. For a single ion of radius *r*, standard electrostatics yields a Born-like equation[48]: $E_{SOLV} = -\frac{Z^2e^2}{2r}\left(1-\frac{1}{\bar{\varepsilon}(1+\bar{\kappa}r)}\right)$, where Ze is the ion charge and $\bar{\kappa} \equiv \left(8\pi e^2 \sum_i Z_i^2 \bar{c}_i / a^3 \bar{\varepsilon} kT\right)^{1/2}$ is the inverse of the Debye length (the a^{-3} term appears because we use dimensionless concentration $\bar{c}$). In a cell system where solvent and monomers have identical size, the ion radius *r* and cell size length *a* are trivially related: $\frac{4}{3}\pi r^3 = a^3$. Moreover, since $\bar{\kappa}r \approx 10^{-1}$ at physiological salt concentration, we may approximate $(1+\bar{\kappa}r)^{-1} \approx 1 - const \cdot \bar{c}^{1/2}$.

The above formula can be generalised to include a spatially inhomogeneous ion distribution. Up to terms proportional to $O(c_\pm^{3/2}(\mathbf{r}))$, we obtain:

$$E_{SOLV} = -\frac{e^2}{2a}\frac{(4\pi/3)^{1/3}}{a^3}\int_V (1-\frac{1}{\varepsilon(\Phi(z))})(c_+(z)+c_-(z)+Z_+^2 c_{Z+}(z))dV$$

, where $c_\pm(\mathbf{r})$ and $c_{Z+}(\mathbf{r})$ are *local* ionic concentrations. We have neglected the ion-ion interaction energy given that it is proportional to $O(c_\pm^{3/2}(\mathbf{r}))$. To a good approximation, the local dielectric permittivity of a fluid can be described as the weighted average of solvent (ε_s) and polymer (ε_p) permittivities

$$\varepsilon(\Phi(\mathbf{r})) \approx \varepsilon_s(1-\Phi(\mathbf{r})) + \varepsilon_p \Phi(\mathbf{r}) \qquad (13)$$

This empirical formula has been experimentally verified for several water-polymer mixtures, including PEG solutions[49,50,51,52]. At low polymer concentrations it is consistent with the Maxwell-Garnett theoretical equation[53,54.]

Adding together the two above contributions, $-TS_{ION}$ and E_{SOLV}, we get a simple formula for the electrostatic energy term of a dilute electrolyte solution

$$E_{ELECT} = \frac{kT}{a^3}\int_V [\ c_+(\mathbf{r})(\log c_+(\mathbf{r})-1) + c_-(\mathbf{r})(\log c_-(\mathbf{r})-1) + c_{Z+}(\mathbf{r})(\log c_{Z+}(\mathbf{r})-1)) - B(1-\frac{1}{\varepsilon(\Phi(\mathbf{r}))})(c_+(\mathbf{r}) + c_-(\mathbf{r}) + Z_+^2 c_{Z+}(\mathbf{r}))\ ]dV \qquad (14)$$

with $B \equiv \frac{e^2(4\pi/3)^{1/3}}{2akT} f$, where $f>1$ is an empirical parameter that takes into account dielectric saturation effects near a strongly charged electrolyte surface[55]. This effect reduces the numerical value of the dielectric permittivity near the ion and, whence, the ion solvation energy. Other specific effects, such as the deviation of the ionic radii from the averaged molecular size *a*, can be also included into *f*. It is worth noticing that in (14) the coupling between polymer, solvent and electrolytes is related to the ion solvation energy through the variation of the dielectric permittivity with polymer concentration. Combining equations (12) and (14), the total energy is the sum of a polymer and electrolyte contribution

$$E_{TOT} = E_{POL} + E_{ELECT} \qquad (15)$$

Ternary system stability

The response of a pseudo-ternary polymer+ions+solvent solution to small thermally-induced fluctuations of polymer and electrolyte concentration can be written as: $\Phi(\mathbf{r}) = \overline{\Phi} + \delta\Phi(\mathbf{r})$, $c_i(\mathbf{r}) = \overline{c}_i + \delta c_i(\mathbf{r})$. We inserted these expressions into (12)-(15) to develop the total free energy as a function of the amplitudes $\delta\Phi(\mathbf{r})$ and $\delta c_i(\mathbf{r})$ up to quadratic terms. We describe fluctuations as a linear combination of sinusoidal waves:

$\delta\Phi(\mathbf{r}) = \sum_{\mathbf{q}} \delta\Phi^{\mathbf{o}}_{\mathbf{q}} \sin \mathbf{q}\cdot\mathbf{r}$ and $\delta c_i(\mathbf{r}) = \sum_{\mathbf{q}} \delta c^{\mathbf{o}}_{i,\mathbf{q}} \sin \mathbf{q}\cdot\mathbf{r}$. Integrating over **r**, the linear terms vanish and we obtain

$$E_{TOT} = E^o_{TOT} + \frac{kTV}{4a^3}\sum_{\mathbf{q}}\left[A_{\overline{\Phi}\overline{\Phi}}(\delta\Phi^o_{\mathbf{q}})^2 + \sum_j\sum_{j'} A_{\bar{c}_j\bar{c}_{j'}}\delta c^o_{j,\mathbf{q}}\delta c^{\mathbf{o}}_{j',\mathbf{q}} + \sum_j A_{\overline{\Phi}\bar{c}_j}\delta\Phi^{\mathbf{o}}_{\mathbf{q}}\delta c^o_{\bar{c}_j,\mathbf{q}}\right] \quad (16)$$

The coefficients $A_{jj'}$ are easily found with the aid of the electroneutrality condition (11):

$$A_{\overline{\Phi}\overline{\Phi}} = \frac{a^2q^2}{24\overline{\Phi}(1-\overline{\Phi})} + \frac{1}{N\overline{\Phi}} + \frac{1}{1-\overline{\Phi}} - 2\chi - 2B\frac{(\varepsilon_p-\varepsilon_s)^2}{\varepsilon^3(\overline{\Phi})}(2\bar{c}_M + Z_+(Z_+ +1)\bar{c}_Z)$$

$$A_{\bar{c}_+\bar{c}_+} = \frac{1}{\bar{c}_M}, \qquad A_{\bar{c}_-\bar{c}_-} = \frac{1}{\bar{c}_M + Z_+\bar{c}_Z}, \qquad A_{\bar{c}_{Z+}\bar{c}_{Z+}} = \frac{1}{\bar{c}_Z}$$

$$A_{\overline{\Phi}\bar{c}_+} = A_{\overline{\Phi}\bar{c}_-} = -B\frac{\varepsilon_p-\varepsilon_s}{\varepsilon^2(\overline{\Phi})}, \qquad A_{\overline{\Phi}\bar{c}_{Z+}} = -Z_+^2B\frac{\varepsilon_p-\varepsilon_s}{\varepsilon^2(\overline{\Phi})}, \qquad A_{\bar{c}_+\bar{c}_-} = A_{\bar{c}_+\bar{c}_{Z+}} = A_{\bar{c}_-\bar{c}_{Z+}} = 0$$

The system is stable against concentration fluctuations when $\det|A| > 0$. The condition $\det|A| = 0$ defines the so-called spinodal curve that divides the phase diagram into stable and unstable regions. Focusing our attention onto macroscopic phase separation, $\mathbf{q} \to 0$, we obtain

$$\frac{1}{N\overline{\Phi}} + \frac{1}{1-\overline{\Phi}} - 2\chi_{eff}(\overline{\Phi}) = 0 \quad (17)$$

$$\chi_{eff}(\overline{\Phi}) = \chi + \begin{cases} 2B\dfrac{(\varepsilon_p-\varepsilon_s)^2}{\varepsilon^3(\overline{\Phi})}\left(\dfrac{B}{2\varepsilon(\overline{\Phi})}-1\right)\bar{c}_M & \bar{c}_Z = 0 \\ BZ_+(Z_++1)\dfrac{(\varepsilon_p-\varepsilon_s)^2}{\varepsilon^3(\overline{\Phi})}\left((Z_+^2-Z_++1)\dfrac{B}{2\varepsilon(\overline{\Phi})}-1\right)\bar{c}_Z & \bar{c}_M = 0 \end{cases} \quad (18)$$

Equation (18) shows that multi-valent ions are more effective in inducing phase

separation. Figure 4 shows the spinodal curve as a function of the Flory interaction parameter $\chi = \chi(T)$ calculated at different monovalent, $\bar{c}_M$, or multi-valent, $\bar{c}_Z$, salt concentrations.

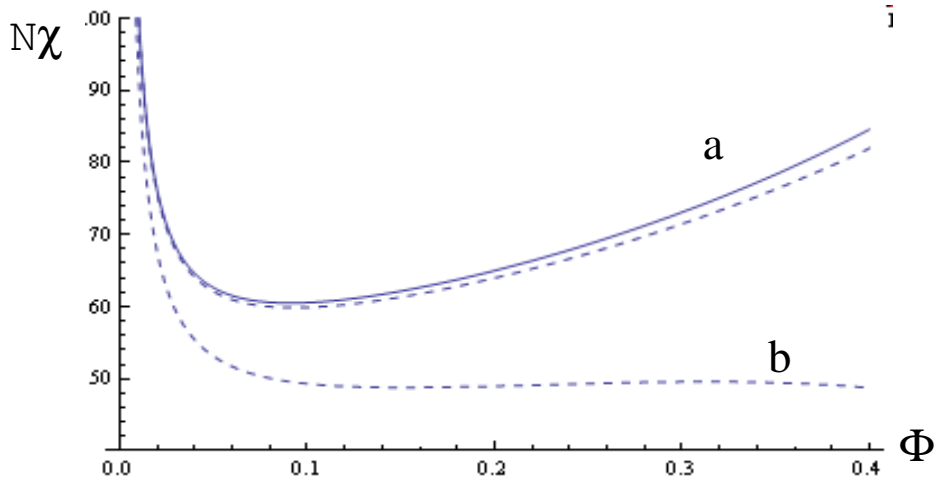

Fig-4 Phase diagram for a polymer-solvent system in the absence (full line) and in the presence (dashed lines) of a constant salt concentration . Curve a) refers to a 0.15 M salt formed by both monovalent anions and cations. Curve b) refers a 0.15 M salt formed by monovalent anions and divalent cations. The sizes of anions and cations were assumed to be identical. In the region below the curves the polymer is homogeneous, while above the curves the system phase separates. Setting *N=100* and $\chi \approx 0.49$, we find that that the fluid becomes unstable to concentration fluctuations in the presence of divalent ions.

We can now make the following conclusions from our simple model:

a) upon increasing the salt concentration ($\bar{c}_M$ or $\bar{c}_Z$), the compatibility between a soluble non-ionic polymer and a polar solvent becomes worse[56,57].

b) the ion effect is larger when solvent and polymer have strongly different dielectric permittivity.

c) Z-valent ions (neutralized by mono-valent counter-ions) are much more effective (about one order of magnitude) than single-valent ions. Experimental data show that trivalent ions, like citrate or phosphate, easily induce phase separation in aqueous polymer solutions[51,52].

d) By maintaining constant ion charge but varying the radius, it can be easily seen that small ions are more effective than big in inducing polymer phase separation (this effect is contained in the coefficient $B \propto a^{-1}$). This is in qualitative agreement with experiments[51,52].

3. POLYMER EFFECT ON THE ADHESION/FUSION RATE

3.1 Art state on PEG-mediated fusion:

Several mechanisms were suggested for how PEG accomplish the fusion process, including: increasing surface tension, absorbing to and crosslinking bilayers, altering the structure and dielectric properties of bulk water, altering the molecular order of the bilayer at the point of contact, producing volume-exclusion-induced aggregation and dehydration, induction of non-bilayer structures, acting as a detergent to disrupt bilayer structure, inducing phase separation that destabilizes the bilayer, producing compressive and then, upon dilution, expansive osmotic stress on membrane vesicles, and containing impurities that disrupted membranes. These proposals and their origins were previously reviewed in detail[58]. **PEG was known to aggregate membranes**, as demonstrated quantitatively by electron microscopy[59] and X-ray scattering[60]. **Some explained this according to surface absorption and cross-linking.** Arnold showed that low molecular weight PEG covalently attached to an alkyl chain that would insert into bilayers, pushed bilayers apart[61], rather than drawing them together. This suggested that absorption of PEG to membrane surfaces was not likely to explain PEG-mediated membrane aggregation, as was confirmed by the observation that PEG could be separated from lipid vesicles by a dialysis membrane and still drive membranes into closer contact[60].

In addition, **Arnold demonstrated that water was excluded from regions of contact between PEG aggregated vesicles** using NMR[62] and electrophoretic mobility[63]. A theoretical treatment supported these experiments by showing that surface exclusion would be expected to provide a membrane aggregating attraction[64], as was then confirmed by direct experiment[65]. Today we know that, aside from producing a thermodynamic force driving close contact between membranes, **PEG also promotes fusion via a positive osmotic pressure that likely helps stabilize fusion intermediates**[66]. **The main effect of PEG on membrane vesicles is believed to be a volume- exclusion aggregation of membranes and dehydration in areas of contact.**

3.2. Establishing new aspects of peg-mediated fusion

Consider two identical large vesicles brought at distance D as shown in Fig.1. When their radii are large, we may neglect curvature effects and consider two parallel surfaces. Classical DLVO (Derjaguin-Landau-Verwey-Overbeek) theory of colloids[67] considers a combination of repulsive electrostatic forces and attractive van der Waals interactions. In biological membranes, other contributions must also be accounted for. For instance, the strongly hydrophilic membrane surface induces short-range repulsive hydration forces due to water ordering at polar interfaces[35,36,68,69,34] and at short distances ligand-receptor bonds may be formed between certain membrane proteins[1,2,3,4] or even by simple divalent cations[5].

We consider the effect of uncharged soluble polymers and focus our attention on the screened electrostatic forces associated with the membrane surface charges. Other forces (like van der Waals and hydration ones) are rather insensitive to polymer addition, constituting a constant background that will be separately added to the total energy.

The system interchanges matter with an external infinite reservoir and after equilibration, the inter-membrane space and the bulk reach different polymer and electrolyte compositions. For the sake of simplicity, we restricted our analysis to temperatures and concentration ranges (low salt and polymer concentrations) , see section 2 ensuring in order avoid any phase separation of polymer and solvent in the bulk fluid. components do not phase-separate. We considered only laterally homogeneous membranes.

Letting $\mathbf{r} = z$ be the distance of a generic point inside the inter-membrane gap from the membrane surface and D to be the gap width, the free energy in the gap region can be partitioned into bulk and surface contributions. Part of the contributions is outlined in the previous section and new contributions will derive by the broader framework that includes the presence of membranes.

a) Bulk contribution

The presence of two charged membranes requires:

a) an energy term related to the electrostatic interactions between the electrolyte's charge distribution and the electrostatic potential:

$\rho(\mathbf{r})\psi(\mathbf{r}) = (e/a^3)(Z_+c_{Z+}(\mathbf{r}) + c_+(\mathbf{r}) - c_-(\mathbf{r}))\psi(\mathbf{r})$ and

b) an energy loss (per unit volume) due to the gradient of the electric field: $-\frac{1}{8\pi}\varepsilon(\mathbf{r})E^2(\mathbf{r})$, where $E(\mathbf{r}) = -\nabla\psi(\mathbf{r})$ is the electric field and $\varepsilon(\mathbf{r}) \equiv \varepsilon(\Phi(\mathbf{r}))$ the dielectric permittivity of the fluid mixture given by (13).

Adding the two terms and integrating over the inter-membrane space, we have

$$E_{FIELD} = \int_V \left[-\frac{1}{8\pi}\varepsilon(\Phi(\mathbf{r}))(\nabla\psi(\mathbf{r}))^2 + \frac{e}{a^3}(Z_+c_{Z+}(\mathbf{r}) + c_+(\mathbf{r}) - c_-(\mathbf{r}))\psi(\mathbf{r})\right]dV \qquad (19)$$

The local ion densities $c_i(\mathbf{r})$ and the potential $\psi(\mathbf{r})$ must be calculated self-consistently.

b) Surface contribution

At the membrane-solution interface (z = 0) the free energy contains additional terms:

a) a term describing the interaction between the charged lipid heads and the surface potential: $\frac{X}{b^2}\int_S e\psi(z)\big|_{z=0}dS$, where X is the (charged lipids)/(total lipids) fraction, b^2 is the surface area of a lipid and e the unit charge ($\sigma = eX/b^2$ defines the membrane's charge density),

b) a term accounting for the interfacial energy of the polymeric solution $\frac{1}{a^2}\int_S \gamma\Phi(z)\big|_{z=0}dS$, γ being the polymer-membrane adhesion energy. Combining these two gives $E_{SUP} \approx \frac{S}{a^2}\left[\,(a/b)^2 Xe\psi(z)\big|_{z=0} + \gamma\Phi(z)\big|_{z=0}\,\right]$ (20)

Next, we combine volume and surface energies and introduce a new variable to describe the polymer volume fraction

$\tau^2(z) = \Phi(z)$ (21)

After simple rearrangement, one finds a compact expression for the total free

$$E_{TOT}/S = \frac{1}{a^2}\Big[\ (a^2/b^2)Xe\psi(z)\big|_{z=0} + \gamma\tau^2(z)\big|_{z=0}\ \Big] +$$

$$\frac{kT}{a^3}\int_0^{D/2}\Bigg[\frac{a^2}{6}\left(\frac{\partial\tau(z)}{\partial z}\right)^2 + F_{FH}(\tau(z)) +$$

$$c_+(z)(\log c_+(z)-1) + c_-(z)(\log c_-(z)-1)$$

$$+ c_{Z+}(z)(\log c_{Z+}(z)-1) - \frac{a^3}{8\pi kT}\varepsilon(\tau(z))\left(\frac{\partial\psi(z)}{\partial z}\right)^2 +$$

$$\frac{e}{kT}(c_+(z)-c_-(z)+Z_+c_{Z+}(z))\psi(z)$$

$$-\Omega(\varepsilon(\tau(z)))(c_+(z)+c_-(z)+Z_+^2c_{Z+}(z))\ \Bigg]dz \qquad (22)$$

where $F_{FH}(\tau(z))$ is the Flory-Huggins component of the polymer energy: $F_{FH}(\tau(z)) \equiv \frac{\tau^2(z)}{N}\log\frac{\tau^2(z)}{N} + (1-\tau^2(z))\log(1-\tau^2(z)) + \chi\tau^2(z)(1-\tau^2(z))$, and $\Omega(\varepsilon(\tau(z))) \equiv B\left(1-\frac{1}{\varepsilon(\tau(z))}\right)$.

Inside the gap, electroneutrality imposes a slight charge excess of electrolyte solution to balance the surface charge density $\sigma = eX/b^2$. Hence, the concentrations $c_j(z)$ must satisfy the constraint

$$\frac{e}{a^3}\int_0^{D/2}\left(Z_+c_{Z+}(z)+c_+(z)-c_-(z)\right)dz = \frac{e}{b^2}X \qquad (23)$$

The equilibrium distribution of the different species is attained when their chemical potentials are identical both in the gap and in the reservoir. This implies a constrained energy minimization procedure as outlined in Appendix A. Specifically, variation of the total free energy with respect to $c_i(z)$ gives

$$\log c_\pm(z) \pm \frac{e}{kT}\psi(z) - \Omega(\varepsilon(\tau(z))) - \mu_\pm = 0 \qquad (24a)$$

$$\log c_{Z+}(z) + \frac{Z_+e}{kT}\psi(z) - Z_+^2\Omega(\varepsilon(\tau(z))) - \mu_{Z+} = 0 \qquad (24b)$$

μ_j being undetermined Lagrange multipliers. Since these relationships must be valid independent of z, we set $z \to \infty$ (bulk solution). Recalling that: $\lim_{z\to\infty} \psi(z) = 0$, $\lim_{z\to\infty} c_j(z) = \bar{c}_j$, and $\lim_{z\to\infty} \varepsilon(\tau(z)) = \bar{\varepsilon}$, we can easily calculate the Lagrange's multipliers μ_j. The final result reads

$$c_{\pm}(z) = \bar{c}_{\pm} \exp\left(\Delta\Omega(\tau(z))\right)\exp\left(\mp \frac{e\psi(z)}{kT}\right) \qquad (25a)$$

$$c_{Z+}(z) = \bar{c}_{Z+} \exp\left(Z_+^2 \Delta\Omega(\tau(z))\right)\exp\left(-\frac{Z_+ e\psi(z)}{kT}\right) \qquad (25b)$$

$\bar{c}_{\pm}$ and $\bar{c}_{Z+}$ being the ion concentrations in the bulk and $\Delta\Omega(\tau(z)) \equiv B\left(\frac{1}{\bar{\varepsilon}} - \frac{1}{\varepsilon(\tau(z))}\right)$. Lastly, minimization of H with respect to $\tau(z)$ and $\psi(z)$, together with use of explicit expressions for $\varepsilon(\tau(z))$ (eq.(13)) and $c_i(z)$ (eqs.(25)), yields a pair of coupled differential equations. By introducing dimensionless potential and polymer concentrations $\psi^* = e\psi(\varsigma)/kT$, $\tau^* = \tau(\varsigma)/\bar{\Phi}^{1/2}$ and dimensionless distance $\varsigma = z/a$, the final equations read

$$\frac{\partial^2 \tau^*}{\partial \varsigma^2} + 6\left(G_o(\tau^*) + G_1(\psi^*, \tau^*)\right)\tau^* = 0 \qquad (26a)$$

$$\frac{\partial}{\partial \varsigma}\left(\varepsilon(\tau^*)\frac{\partial \psi^*}{\partial \varsigma}\right) = \bar{\varepsilon}\bar{\kappa}^2 a^2 \exp\left(B\left(\frac{1}{\bar{\varepsilon}} - \frac{1}{\varepsilon(\tau^*)}\right)\right)\sinh(\psi^*) \qquad (26b)$$

where $\bar{\kappa} \equiv \left(8\pi e^2 \bar{c}/a^3 \bar{\varepsilon} kT\right)^{1/2}$ is the Debye length of a homogeneous mixed solvent and

$$G_0(\tau^*) \equiv \log\left(\frac{1-\bar{\Phi}\tau^{*2}}{1-\bar{\Phi}}\right) + 2\chi\bar{\Phi}(\tau^{*2} - 1) - \frac{2}{N}\log\tau^* \qquad (27a)$$

The term

$$G_1(\psi^*,\tau^*) \equiv (\varepsilon_p - \varepsilon_s)\left(\frac{akT}{8\pi e^2}\left(\frac{\partial\psi^*}{\partial\varsigma}\right)^2 + \frac{2B}{\bar{\varepsilon}^2}\bar{c}_M\left[\frac{\bar{\varepsilon}^2}{\varepsilon^2(\tau^*)}\exp\left(B\left(\frac{1}{\bar{\varepsilon}} - \frac{1}{\varepsilon(\tau^*)}\right)\right)\cosh(\psi^*) - 1\right]\right) \quad (27b)$$

describes the is a coupling term between the electrostatic potential and polymer concentration. Specifically, the gradient term in (27b) is related to the dielectric inhomogeneities of the medium, while the B- dependent term describes salting-out effects linked to the different solvent and polymer dielectric permittivities. The salting-out effect appears also in the second term of the right-hand side of equation (27b).

In (27b) we disregarded terms depending on $c_{z+}(\varsigma)$. Despite the relevant role of multivalent ions in screening the electrostatic potential, the ratio between the mono- and divalent ion concentration in biological fluids is as small as 10^{-5}, enabling us to neglect the role of $c_{z+}(\varsigma)$ on ψ^* and τ^*. This approximation, however, is no longer permissible at the membrane-water interface $\varsigma = 0$ because of the large binding constant of multi-valent ions with charged membranes. This point will be thoroughly discussed in the next section where the effect of bound ions on the electrostatic and polymer profiles will be investigated.

With (26a) we can calculate the inhomogeneous polymer distribution $\Phi(\varsigma) = \bar{\Phi}\tau^{*2}$. If we omit in (26a) the ion-polymer coupling term $G_1(\psi^*,\tau^*)$, in (27a), develop the Flory-Huggins polymer energy up to τ^{*4} and neglect the small term proportional to N^{-1}, we recover the de Gennes equation for the concentration profile of a semi-dilute polymer near a wall[43]: $\frac{\partial^2\tau^*}{\partial\varsigma^2} + A(1-\tau^{*2})\tau^* = 0$, with $A \equiv 6(1-2\chi)\bar{\Phi}$. Equation (26b) is nothing but a generalized Poisson-Boltzmann equation and at constant polymer concentration ($\tau^* \to 1$) it reduces to the familiar expression: $\frac{\partial^2\psi^*}{\partial\varsigma^2} = \bar{\kappa}^2\sinh(\psi^*)$.

The above equations must satisfy proper boundary conditions. In the case of two identical surfaces, (4Ab) of Appendix A gives

$$\partial\psi^*/\partial\varsigma\big|_{\varsigma=D/2a} = \partial\tau^*/\partial\varsigma\big|_{\varsigma=D/2a} = 0 \quad (28a)$$

More interesting is the behaviour of ψ^* and τ^* at the interface $\varsigma = 0$. From (4Aa) we get

$$\varepsilon(\tau^*|_{\varsigma=0}) \cdot \left.\frac{\partial \psi^*}{\partial \varsigma}\right|_{\varsigma=0} = \frac{4\pi e^2}{kTa}\left(\frac{a}{b}\right)^2 X \qquad (28b)$$

$\sigma = eX / b^2$ being the membrane surface charge density. Analogously, from (4Aa) we obtain a boundary to the polymer profile at $\varsigma = 0$

$$\left.\frac{\partial \tau^*}{\partial \varsigma}\right|_{\varsigma=0} = \frac{6\gamma}{kT}\tau^*|_{\varsigma=0} \qquad (28c)$$

a formula connecting the interfacial polymer concentration to the adhesion energy γ. The differential equations (26a,b), subjected to the boundary conditions (28a-c), are the basic tools to explore the effect of neutral polymers on the ion distribution and membrane-membrane interactions.

3.2.1. Approximate limiting cases

The procedure developed so far yields two coupled non-linear differential equations. They can be solved only numerically as will be shown in the next section. Asymptotic formulas are obtained in a few relevant cases.

Long-distance limit

When the distance D between the two opposing surfaces is much larger than R_G ($\approx N^{3/5}$), the polymer concentration in the central region of the membrane gap is similar to that of the bulk. So, when $\varsigma \approx D / 2a >> 1$ we can write the scaled polymer concentration as $\tau^* = 1 - \eta(\varsigma)$, with $\eta(\varsigma) << 1$. The same reasoning applies to the potential ψ_o^* that must be very small. Inserting $\tau^* = 1 - \eta(\varsigma)$ into (26a,b) and neglecting higher order terms in $\eta^2(\varsigma)$, we may decouple the system of equations. Proceeding as shown in the Appendix B, we obtain

$$\Phi(z) \approx \overline{\Phi}(1-\Theta(e^{-2Az/a}+e^{-2A(D-z)/a}))^2 + O(e^{-2\bar{\kappa}z}) \qquad (29)$$

Θ being of order $48\frac{\varepsilon_p-\varepsilon_s}{\bar{\varepsilon}}(1-2\chi)\overline{\Phi}\Gamma^2\left(1-\frac{2B}{\bar{\varepsilon}}\right)e^{-\bar{\kappa}D/2}\bar{c}_M$. Physically, the polymer profile in the distal region of the gap reaches a maximum and decays with a characteristic length of $a/A \equiv 1/\sqrt{6(1-2\chi)\overline{\Phi}}$ that depends on the polymer properties alone (mean concentration $\overline{\Phi}$ and non-ideal mixing parameter χ). Near the walls the polymer profile is mainly ruled by the dimensionless Debye length $1/\bar{\kappa}a$.

Short-distance limit

When $D<R_G$ the situation becomes simpler. According to the Asakura-Oosawa theory[70], polymer chains ought to be totally excluded from the gap because of the chains' entropy-driven deformation energy.

However, there is a concomitant migration of ions from the bulk to the gap due to the combined effects of electrostatic attraction by the charged walls coupled to a dielectric-mediated ionic flux from low (bulk) to high (gap) dielectric permittivity. Therefore, the equilibrium ion concentration inside the gap is given by (26b), provided the dielectric permittivity within the gap is replaced by that of the pure solvent. Accordingly, the modified Poisson-Boltzmann equation (26b) reduces to

$$\frac{\partial^2\psi^*}{\partial\zeta^2} = \kappa_{eff}^2 a^2 \cdot \sinh(\psi^*) \qquad (30)$$

where the effective Debye length has been properly renormalized to account for salting-out effects: $\kappa_{eff}^2 \equiv \bar{\kappa}^2\frac{\bar{\varepsilon}}{\varepsilon_s}\exp\left(B\left(\frac{1}{\varepsilon_s}-\frac{1}{\bar{\varepsilon}}\right)\right)$.

3.2.2. Self-regulating surface charges

We have seen that, despite the greater effectiveness of multi-valent ions in screening the electrostatic potential and disfavouring the solvent-polymer compatibility,

they should have a modest role in polymer-assisted membrane fusion because of their smaller concentration at physiological conditions. The situation is reversed when we consider the membrane surface. Here the local concentration of cations such as calcium and magnesium is high and comparable to that of monovalent ions because divalent cations form tight complexes with the phosphate or carboxylic groups of lipid heads[71,72,73,74].

Regulation of the surface charges is described by introducing a few additional contributions to the surface energy:

Ion binding energy. Binding of a Z-valent ion to a charged membrane neutralizes Z_+ lipid heads. Letting θ to be the unknown fraction of neutralized sites ($0<\theta<1$), the surface concentration of a Z-valent ion is $\frac{X}{Z_+ b^2}\theta$, where X is the fraction of charged lipids and b^2 the lipid surface area. Therefore, the binding energy reads: $-\frac{X}{Z_+ b^2}\int_S \theta E Z_+ dS$, where $-E$ is the ion-lipid binding energy per single bond.

Entropy term. The entropy of mixing among occupied and vacant sites over the membrane surface takes the standard form: $\frac{X}{Z_+ b^2}\int_S kT\theta\log\theta+(1-\theta)\log(1-\theta))dS$.

Surface electrostatics. Due to the partial neutralization of the charged lipids by tightly adsorbed ions, the membrane surface density is lowered from the initial value σ to $\sigma(1-\theta)$ (with $\sigma \equiv eX/b^2$). Thus, the electrostatic energy variation upon ion binding reads: $\int_S \sigma(1-\theta)\psi(z)\big|_{z=0} dS$.

Summing up, the energy terms a)-c), and introducing the polymer-surface interaction, we generalize equation (20) obtained for non-adsorbing membrane surfaces

$$E_{SUP} = \frac{S}{a^2}\left[(a^2/b^2)Xe(1-\theta)\cdot\psi(z)\big|_{z=0} + \gamma\tau^2(z)\big|_{z=0} + F(\theta) \right] \qquad (31)$$

where: $\frac{XkTa^2}{Z_+ b^2}\left[\theta\log\theta+(1-\theta)\log(1-\theta) - \frac{Z_+ E}{kT}\theta \right]$. Calculating the chemical potential of an adsorbed ion by minimizing (31) with respect to θ, equating the surface

and bulk chemical potentials and introducing the dimensionless variables $\psi^* = e\psi(\varsigma)/kT$, $\tau^* = \tau(\varsigma)/\overline{\Phi}^{1/2}$ and $\varsigma = z/a$, we get

$$\frac{\theta}{1-\theta} = \bar{c}_{z^*} K_{eff}(\theta) \qquad (32)$$

From (32) we can obtain θ numerically. It is convenient to write the effective binding constant of a Z-valent ion as

$$K_{eff}(\theta) \equiv K_o \exp\left(Z_+ \psi^*\big|_{\varsigma=0} + Z_+^2 B\left(\frac{1}{\bar{\varepsilon}} - \frac{1}{\varepsilon_s}\right)\right) \qquad (33)$$

where K_o>1 is the intrinsic ion-membrane binding constant measured in pure solvent at zero surface potential (K_o can be assimilated to the experimental ion binding constant when the charged sites are dissolved into a sea of neutral lipids). The exponential term in (33) describes the electrostatic effect of the charged lipid headgroups on the ion binding. Unfortunately, no analytical expressions are available for the surface potential ψ^* in mixed solvents. However, by numerically calculating $\psi^*\big|_{\varsigma=0}$ for different values of the fraction of charged lipids concentration X, and interpolating the obtained curves with the expansion $\psi^*\big|_{\varsigma=0} = A_1 + A_2\theta + A_3\theta^2 +$ …, we obtain the unknown coefficients A_j. This procedure transforms (32) into a Frumkin type equation[75].

$$\frac{\theta}{1-\theta} = \bar{c}_{z^*} K_o \exp(Z_+(A_1 + A_2\theta + A_3\theta^2 + ...)) \qquad (34)$$

which is numerically solved for θ. Using these values for surface charge neutralization, we can use (26a,b) to calculate the polymer concentration and the electrostatic potential by replacing the fraction of charged lipids X by $X(1-\theta)$ in the boundary condition (28b). Numerical results will be briefly described in section 5.

Although the bulk concentration of multivalent ions is much smaller than that of monovalent ones, their relative concentrations near the membrane surface are similar because of the stronger binding of multivalent cations.

3.2.3. Interaction between two charged surface in mixed electrolyte-polymer-solvent fluid.

Once the electrolyte and polymer concentration profiles inside the gap have been calculated, we can derive the inter-membrane pressure. The total pressure P between two identical planar charged surfaces embedded in a multi-component fluid has been calculated by several authors. Andelman and co-workers obtained

$$-P=\frac{1}{8\pi}\left(\varepsilon+\sum_{i=1}^{M}\frac{\partial\varepsilon}{\partial n_i}n_i\right)\left(\frac{\partial\psi^*}{\partial\varsigma}\right)^2+h-\sum_{i=1}^{M}\frac{\partial h}{\partial n_i}n_i \qquad (35)$$

for a mixture that contains M different species[89] . n_i is the concentration of each component, h is the grand potential without any explicit ψ^*-dependent electrostatic interactions (in our notation $h=\lim_{\psi(z)\to 0} H/S,$ with H given by (1B)). Here n_i are polymer concentration $\Phi(z)=\tau^2(z)$ and electrolyte concentrations $c_{\pm}(z)$. Using the analytical expression for the dielectric permittivity given by (11), we find

$$-P=\frac{kT}{a^2}\left[\ P_1+P_2+P_3+P_4\ \right] \qquad (36)$$

$$P_1=\frac{1}{8\pi}\left(\varepsilon_s+2(\varepsilon_p-\varepsilon_s)\Phi\right)\left(\frac{\partial\psi}{\partial z}\right)^2 \qquad P_3=\Phi(1-\tfrac{1}{N})+\log(1-\Phi)+\chi\Phi^2$$

$$P_2=-(c_+ + c_-) \qquad P_4=B\frac{\varepsilon_p-\varepsilon_s}{\varepsilon^2(\Phi)}\Phi(c_+ + c_-)$$

The first term, P_1, is the electrostatic pressure arising from the Maxwell stress tensor, the second one, P_2, originates from the entropy of mixing of positive and negative ions. This term is basically the Van't Hoff osmotic pressure originating from a gas of charged particles. The third term, P_3, describes the Van't Hoff osmotic pressure of a polymer solution. Finally, the last term, P_4, describes an explicit coupling term between electrolyte and polymer concentrations.

To find the net interaction between the plates, we subtract the reservoir pressure from the total pressure (36)

$$\delta P = P - \overline{P} \qquad (37)$$

The analytical expression for the polymer-induced osmotic pressure of the reservoir, $\overline{P}$, is calculated from (37) by taking the limit $z \to \infty$. A simplification is obtained from the conservation of pressure for a given separation D. If we evaluate the pressure at the midplane z=D/2, field and polymer gradient terms vanish by symmetry. Finally, by using the relationship (26) between electrolyte concentration and potential ψ, we find

$$\delta P = -\frac{kT}{a^3}\Big[(\Phi|_{D/2} - \overline{\Phi})(1-\tfrac{1}{N}) + \log\frac{1-\Phi|_{D/2}}{1-\overline{\Phi}} + \chi(\Phi^2|_{D/2} - \overline{\Phi}^2) -$$

$$2\overline{c}_M\left(\left(1-B\frac{\varepsilon_p-\varepsilon_s}{\varepsilon^2(\Phi|_{D/2})}\Phi|_{D/2}\right)\exp\left(B\left(\frac{1}{\overline{\varepsilon}}-\frac{1}{\varepsilon(\Phi|_{D/2})}\right)\right)\cosh\left(\frac{e\psi|}{kT}\Big|_{D/2}\right)-\left(1-B\frac{\varepsilon_p-\varepsilon_s}{\overline{\varepsilon}^2}\overline{\Phi}\right)\right)\Big] \qquad (38)$$

In order to prove the correctness of the interplates pressure (36) we first expanded the pressure in power series of Φ (a correct procedure in the semi-dilute regime $\Phi<<1$), then, neglected the polymer-related salting-out effects, B=0. These approximations led to a well known result:

$$-\delta P_3 \approx \frac{kT}{a^3}\Big[\frac{1}{N}(\Phi|_{D/2} - \overline{\Phi}) + \tfrac{1}{2}\nu(\Phi^2|_{D/2} - \overline{\Phi}^2) - 2\overline{c}_M(\cosh(\frac{e\psi|}{kT}\Big|_{D/2}) - 1) \Big], \quad \text{with}$$

$\nu \equiv 1-2\chi$. This classical relationship shows that in ideal systems the pressure is the sum of an ion and a polymer contribution, any polymer-ion coupling just renormalize the polymer concentration $\Phi|_{D/2}$ and electrostatic potential $\psi|_{D/2}$ at the midplane.

Limiting the analysis to the semi-dilute regime, $\Phi<<1$, we may expand the pressure in power series of Φ. Then, neglecting salting-out effect on polymer distribution, B=0, we recover a well known result showing the independent contributions of osmotic and electrostatic forces:

$$-\delta P_3 \approx \frac{kT}{a^3}\Big[\frac{1}{N}(\Phi|_{D/2} - \overline{\Phi}) + \tfrac{1}{2}\chi(\Phi^2|_{D/2} - \overline{\Phi}^2) - 2\overline{c}_M(\cosh(\frac{e\psi|}{kT}\Big|_{D/2}) - 1) \Big], \quad \text{with}$$

$\nu \equiv 1-2\chi$, a result that proves the correctness of our approach.

Summing up, the addition of a neutral polymer to a system with interacting charged membranes gives rise to: a) ions-modulated depletion forces and b) modified polymer-modulated electrostatic repulsion. These two effects are intimately related,

especially when the polymer and solvent permittivities differ to a large extent (strong salting-out effects). , however, are closely related since both polymer concentration $\Phi|_{D/2}$ and electrostatic potential $\psi|_{D/2}$ are strongly coupled. Therefore, the parameter $\delta P = (\delta P - \delta P|_{\bar{\Phi}=0})$ is the most useful in describing the effect of added polymer.

In chapter 5 results will be discussed and compared with our computational findings.

4. COMPUTATIONAL APPROACH

4.1 Coarse-Grained approach

Lipid molecules play an important role in a multitude of chemical and biological processes. By virtue of their amphiphilic architecture, lipids form the basic building blocks of the biological membranes. Besides the standard role exerted by the lipid bilayer which acts as a selective permeable barrier between the internal and external medium, membranes are also involved in collective phenomena that change their own topology by fusion, lysis, budding, or pore formation. These collective phenomena are involved in fundamental biological processes such as fertilization, synaptic release, intracellular traffic, and viral infection.

Much of the difficulty in obtaining a microscopic view of these long-range cooperative phenomena typical of a visco-elastic system, can be traced to the length and time scales on which these processes occur a few tens of nanometers and milliseconds. These scales are not approachable to direct experimental observation or a fully atomistic theoretical study.

Coarse graining models attempt to describe the large scale phenomena by lumping a small number of atoms into an effective particle[76]. **The reduced number of degrees of freedom and the softer interactions on the coarsened scale lead to a significant computational speed up with the consequence that larger system and longer time scales are accessible**. This makes possible the study of collective phenomena in membranes, a study not possible via ab initio methods now. However, the loss of chemical detail limits some of the predictive power of coarse-grained models.

The question that remains is just what are the relevant interactions necessary to bring about the collective phenomena observed in experimental system.

Within the framework of minimal models, one can start with a simple model and successively augment it with additional interactions until the phenomena of interest is captured. This method provide insight into which interactions, on the length scales of a few atomic units, are necessary to bring about collective behavior in membranes and contributes to identifying those mechanisms that underlie the phenomena and the degree of universality.

For this reason, starting from a recent model of Cooke et al.[77] and with the use of a versatile software like ® Espresso allowing me to freely change the code according my needs, **in my first year of doctorate I refined and changed the lipids parameterization in order to obtain a better representation of soft matter self-aggregates like flat bilayers and vesicles**. After a preliminary assessment, **I then tested the consistency of the model with a series of biologically and chemically significant examples**.

We realized that the lack of assembled membranes made up by lipids already parameterized required an extensive work, out of our prefixed time terms.

In addition, it is higher the probability to amplify the error committed for approximations because of the high magnification of details.

During the second year, in order to catch the high complexity of the investigated system, we reputed more adequate the use of a "systematic" coarse grained approach[80] in the framework of the Martini parameterization and the suitable Gromacs package.

4.1.1 Martini philosophy

Martini model[80] has also been developed in close connection with more detailed atomistic models; however, the philosophy of coarse graining approach is different. Instead of focusing on an accurate reproduction of structural details at a particular state point for a specific system, they aim for a broader range of applications without the need to re-parameterize the model each time. They do so by extensive calibration of the building blocks of the coarse grained force field against thermodynamic data, in particular oil/water partitioning coefficients. Processes such as lipid self-assembly, peptide membrane binding or protein-protein recognition depend critically on the degree to which the constituents partition between polar and not polar environments. The use of a consistent strategy for the development of compatible coarse grained and atomic level force fields is of additional importance for its intended use in multi-scale applications[78] .

4.1.2. The Model

The model is based on a four-to-one mapping, i.e., on average four heavy atoms are represented by a single interaction center. For ring structures a different mapping is introduced, as will be explained below. In order to keep the model simple, it considers only **four main types of interaction sites: polar (P), nonpolar (N), apolar (C), and charged (Q)**. Each particle type has a number of subtypes, which allow for a more accurate representation of the chemical nature of the underlying atomic structure. The total number of subtypes has increased from 9 to 18. Within a main type, **subtypes are either distinguished by a letter denoting the hydrogen-bonding capabilities** (d) donor, a) acceptor, da) both, 0) none), **or by a number indicating the degree of polarity** (from 1, low polarity, to 5, high polarity).

		Q				P					N				C				
	sub	da	d	a	0	5	4	3	2	1	da	d	a	0	5	4	3	2	1
Q	da	O	O	O	II	O	O	O	I	I	I	I	I	IV	V	VI	VII	IX	IX
	d	O	I	O	II	O	O	O	I	I	I	III	I	IV	V	VI	VII	IX	IX
	a	O	O	I	II	O	O	O	I	I	I	I	III	IV	V	VI	VII	IX	IX
	0	II	II	II	IV	I	O	I	II	III	III	III	III	IV	V	VI	VII	IX	IX
P	5	O	O	O	I	O	O	O	O	O	I	I	I	IV	V	VI	VI	VII	VIII
	4	O	O	O	O	O	I	I	II	II	III	III	III	IV	V	VI	VI	VII	VIII
	3	O	O	O	I	O	I	I	II	II	II	II	II	IV	IV	V	V	VI	VII
	2	I	I	I	II	O	II	II	II	II	II	II	II	III	IV	IV	V	VI	VII
	1	I	I	I	III	O	II	II	II	II	II	II	II	III	IV	IV	IV	V	VI
N	da	I	I	I	III	I	III	II	II	II	II	II	II	IV	IV	V	VI	VI	VI
	d	I	III	I	III	I	III	II	II	II	II	III	II	IV	IV	V	VI	VI	VI
	a	I	I	III	III	I	III	II	II	II	II	II	III	IV	IV	V	VI	VI	VI
	0	IV	IV	IV	IV	IV	IV	IV	III	III	IV	IV	IV	IV	IV	IV	IV	V	VI
C	5	V	V	V	V	V	V	IV	IV	IV	IV	IV	IV	IV	IV	IV	IV	V	V
	4	VI	VI	VI	VI	VI	VI	V	IV	IV	V	V	V	IV	IV	IV	IV	V	V
	3	VII	VII	VII	VII	VI	VI	V	V	IV	VI	VI	VI	IV	IV	IV	IV	IV	IV
	2	IX	IX	IX	IX	VII	VII	VI	VI	V	VI	VI	VI	V	V	V	IV	IV	IV
	1	IX	IX	IX	IX	VIII	VIII	VII	VII	VI	VI	VI	VI	VI	V	V	IV	IV	IV

Table 1. Level of interaction indicates the well depth in the LJ potential. The LJ parameter σ= 0.47 nm for all interacion levels except level IX for which σ = 0.62 nm. Four different CG sites are considered: charged (Q), polar (P), nonpolar (N), and apolar (C). Subscripts are used to further distinguish groups with different chemical nature: 0, no hydrogen-bonding capabilities are present; d, groups acting as hydrogen bond donor; a, groups acting as hydrogen bond acceptor; da, groups with both donor and acceptor options; 1-5, indicating increasing polar affinity (adapted from 80).

4.2. Objective

The objective of our simulations is to follow the release of the polymer from the intermembrane space, which should be accompanied by an increased concentration of calcium ion. The greater number of divalent calcium ions in the intermembrane space should favor the subsequent formation of bridges between the two membranes in close opposition through the formation of Cis complexes with calcium. These initial contacts should laterally expand leading to a complete adhesion of the membranes.

In order to verify the salting out properties of the polymer we will use, as control, the system with charged membranes but without polymer and finally the neutral system of DPPC in presence of polymer.

We want to explore the potentiality of this approach in order to investigate and capture biologically relevant cooperative phenomena like membrane adhesion/fusion by a combined use of coarse grained models and high computational performance.

4.3. Computational details

We start by introducing the computational model we used in study. In our simulations, we used the coarse-grained Martini parameterization[79] .

The following systems were simulated:

1) a system consisting of only water and polyethylene glycol (PEG) (10% of volume)
2) the same system as the previous one in the presence of salt (sodium chloride / calcium chloride) at two different concentrations, 0.1 M and 0.4 M respectively.

To study the effects of polymer on the adhesion of charged membranes, we set up three different coarse-grained systems:

a. Two flat bilayers made up of 3200 molecules of negatively charged palmitoyl-oleoyl-phosphatidylglycerol (POPG). The bilayers were inserted in a water box (500000 water beads) in the presence of 0.1 M sodium chloride (7241 sodium ions, 3073 chlorine ions). The solution contained also calcium ions 0.01 M (1500 atoms) and

10% volume of inert uncharged polymer chains of polyethylene glycol (PEG (1200 molecules). The degree of polymerization of polymerization was 37. The solution was electroneutral.

b. The same system without PEG was used as a reference system.

c. The results obtained from the above systems with charged lipids were compared with those using neutral lipids. For that, we had a similar setup made up of 3200 molecules of neutral dipalmitoylphosphatidylcholine (DPPC). Water, PEG and salt were added as above (3073 sodium ions, 6073 chlorine ions and 1500 calcium ions).

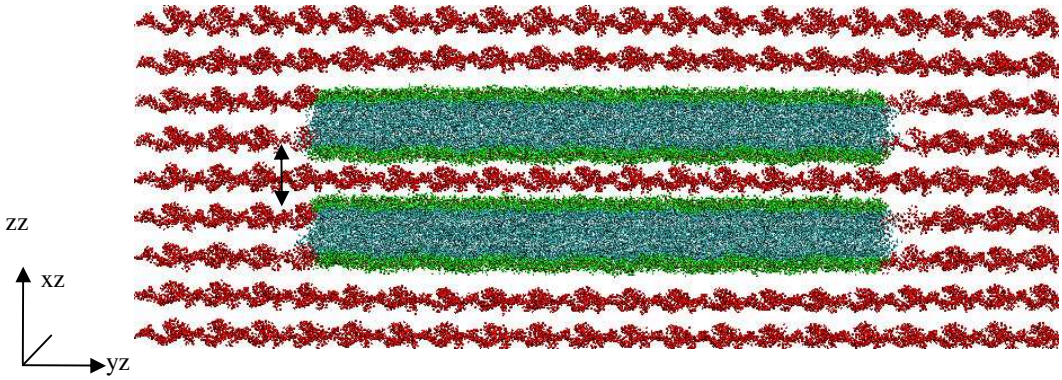

Fig-5 Initial setup used in simulations of POPG membranes (green and light blue) and PEG (red). . Water and ions are not shown in the snapshot. The distance between the two membranes is D.

The membrane has free borders along the y-axis in order to promote flux of ions and PEG inside or outside the membrane space (Fig.5). For this we constrained the lipids' centers of mass. Periodic boundaries conditions are applied to the three dimensions of the box.

After the investigation of the systems at the steady state in different conditions, we want to follow them in a dynamic way. To this aim, we released the constraints and let the membranes free to fluctuate. In this way we could explore the effects of polymer on the adhesion/fusion of charged membranes.

To set up the new three different coarse-grained systems (d, e, f, g) we resized the box in order to have infinitive membranes in the three dimensions, where periodic boundary conditions were applied, keeping the same ratios of species concentration as in the systems a, b and c.

d. Two flat bilayers made up of 5304 molecules of negatively charged palmitoyl oleoyl-

phosphatidylglycerol (POPG). The bilayers were inserted in a water box (141917 water beads) in the presence of 0.1 M sodium chloride (5448 sodium ions, 824 chlorine ions). The solution contained also calcium ions 0.01 M (340 atoms) and 10% volume of inert uncharged polymer chains of polyethylene glycol (PEG (10%). The degree of polymerization of polymerization was 37. The solution was electroneutral.

e. The same system as (d) but with an increased amount of PEG (30%).
f. The same system without PEG was used as a reference system (d).
g. The results obtained from the above systems with charged lipids were compared with those using neutral lipids. For that, we had a similar setup made up of 5300 molecules of neutral dipalmitoylphosphatidylcholine (DPPC). Water, PEG and salt were added as above (2760 sodium ions, 3440 chlorine ions and 340 calcium ions, 10% of PEG).

A pore crossing the two apposed membranes was generated along the z axes using the mffa potential[80] to permit the diffusion of water, ions and polymer through it while the membranes are approaching (Fig.6).

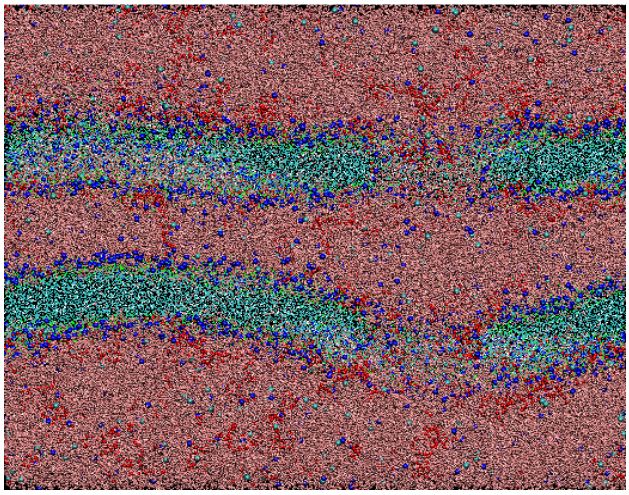

Fig.6 Two flat charged membranes (cyan) crossed by a pore, in presence of water (pink beads), salt (in blue sodium ions and cyan chlorine), calcium ions (light blue) and polymer (red beads).

The essence of CG models is to use short-ranged potential in order to be computationally efficient. This allowed us to explore cooperative effects of considerable entity like the exclusion of polymer from the interlamellar region between two hypothetical giant vesicles.

Electrostatic interactions, however are long ranged. Recently Martini group

parameterized a new polarizable coarse-grained water model in order to reproduce the dielectric screening of bulk water[81].

All the previous systems (d, e, f, g), now resized, were then simulated in presence of polarizable water where the long-range effects are expected to be more realistic considering the explicit screening (the dielectric constant ε_r =2.5). After a long equilibration of 500ns, in this way we expected to follow a dynamic phenomenon finely dependent by a good description of the electrostatics component. We performed check simulations in order to verify the descriptive ability of the model in conformity with previous observations (data not reported).

Simulations were performed by version 4.0.7 of the GROMACS simulation package[82] and the MARTINI 2.0 force field was used for lipids**Errore. L'origine riferimento non è stata trovata.** and PEG[83].

The Berendsen weak coupling temperature and pressure coupling algorithms[84] were utilized with coupling constants of 0.3 *ps* and 3.0 *ps*, respectively. Lipids , and water and ions were separately coupled to a heat bath. The Lennard-Jones potential was smoothly shifted to zero between 9 and 12 Å. For electrostatics, we used the smoothly shifted and truncated Coulomb potential which was smoothly shifted to zero between 0 and 12 Å.

Each system was minimized by steepest descent algorithm after the adding each of the molecular species and then equilibrated in NpT ensemble for 500 *ns* prior to data collection. After that time, indeed the density profiles of the species (ions and polymer) appear stabilized. The time step was set to 0.025 *ps* when polymer was not present and to 0.010 *ps* for the system in presence of polymer[83]. The simulation time was 1 µm for each of the system.

5. RESULTS AND DISCUSSION

5.1. Pseudo-ternary system polymer+ions+ solvent

We used MD simulations to study the qualitative behavior of our simple analytical model described in sec 3. Figure 7 shows a comparison of two snapshots of a PEG solution (10%) in the presence of mono- or divalent salts at the same 0.4 M concentration. As Fig. 7 shows, ions are mostly dissolved inside water-rich fluctuating patches (black regions). In agreement with the results of the mean field model Fig. 4, divalent cations (panel c) are more excluded from the polymer-rich domains. To support our qualitative observations, we also reported the tendency to form polymer/salt clusters enriched in the different systems (fig 8).

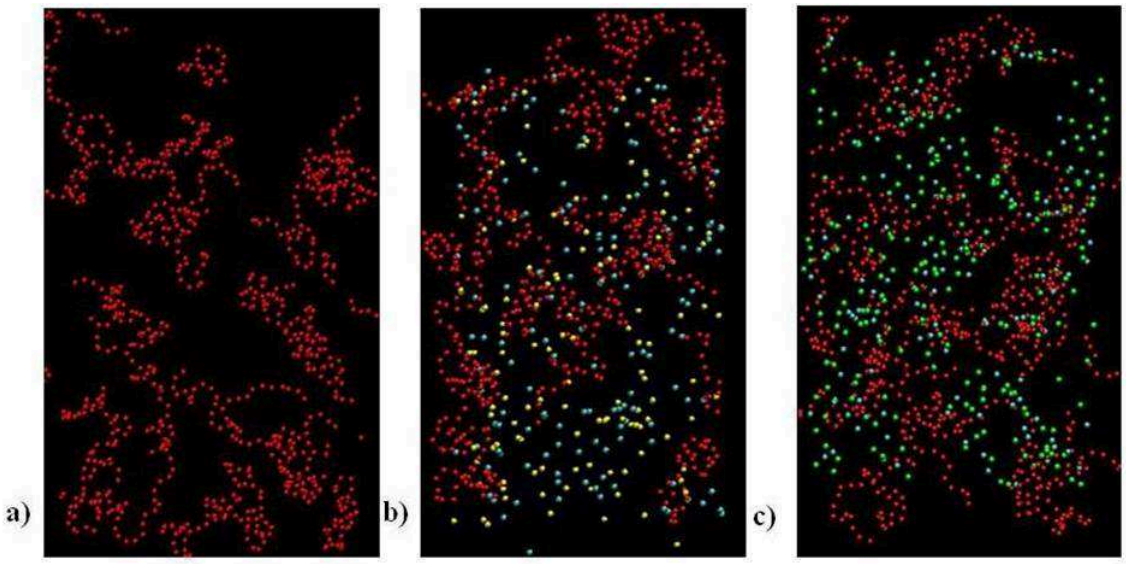

Fig. 7 a) PEG solution (10%) without salt; b) PEG solution (10%) in the presence of mono-valent salt (NaCl, total ions concentration 0.4 M); c) PEG solution (10%) in the presence of divalent-salt ($CaCl_2$, total ions concentration 0.4 M, identical to that of panel b) Notice the increased ion concentration inside fluctuating water pools (black regions).

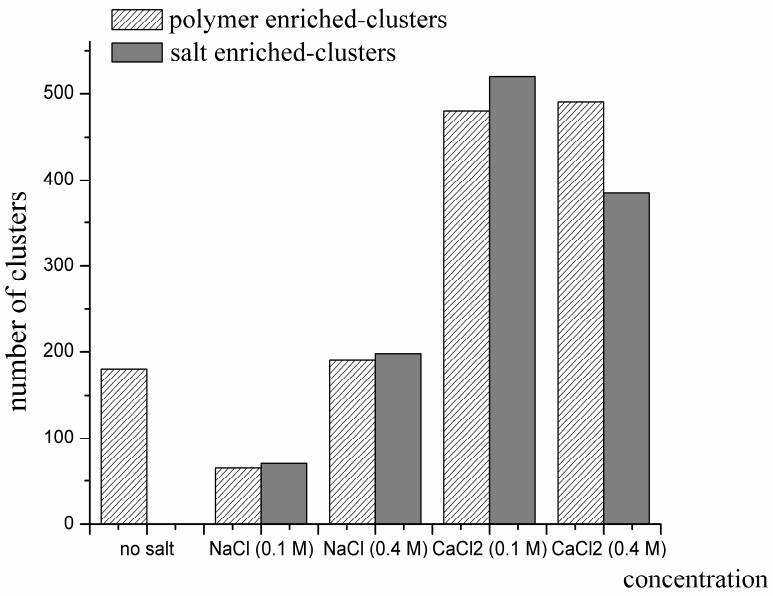

Fig. 8 The number of polymer-enriched clusters (dashed texture) and salt-enriched clusters (gray) at different conditions as calculated by our *MD* simulations: a) PEG solution (10%) without salt, b) PEG solution (10%) in the presence of monovalent salt (0.1 M NaCl), c) PEG solution (10%) in the presence of mono-valent salt (0.4 M NaCl), d) PEG solution (10%) in the presence of divalent salt (0.1 M $CaCl_2$) ; e) PEG solution (10%) in the presence of divalent salt (0.4 M $CaCl_2$).

Despite the greater effect of multi-valent ions in worsening polymer-solvent compatibility, the low divalent cation concentration in biological fluids[85] makes a direct influence on polymer-solvent mixing properties unlikely. We will show, however, that divalent cations still play a key role in membrane adhesion.

The above results motivated us to investigate a different model for polymer-induced adhesion of charged membranes based on non-additive osmotic and electrostatic forces. Such an idea is not entirely new. After some past attempts carried out by us on a single surface in contact with a polymer-containing electrolyte solution[86], more recently Croze and Cates investigated a similar model involving two charged surfaces placed at a finite distance[87], but they neglected the polymer-induced salting-out effect. As shown by the above equations, however, salting-out have an important role in determining the behaviour of polymer-electrolyte solutions. A related, but different model has been

developed by Ruckenstein. He investigated the coupling between double layer and depletion forces induced by rigid spheres[88]. More recently, similar approaches have been developed by Andelman and collaborators[89,90] in studying electrostatic forces in monomeric mixed solvents, while coupled electrostatic and depletion forces have been suggested to explain the anomalous scattering properties of colloidal suspensions[91].

5.2. Two charged membranes interacting with a pseudo-ternary system polymer+ ions+ solvent

The formulas developed so far yield simple relationships between the adhesion rate and properties of lipid membranes. Here we solve them numerically using the following parameters: The initial equilibrium inter-membrane distance was set to $D = 2\times10^{-9} m$. Surface charge density was set to $\mathrm{X}\sigma$, where $\sigma = e\cdot(0.8)^{-2}\times10^{-18} m^{-2}$ corresponds to one elementary charge per area and X is the fraction of negatively charged lipids. The binding constant K_o of divalent cations was set to 30 M^{-1}. This value was chosen since it reproduces the calcium binding constant to negative phosphatidylserine lipid bilayers in water. Mono-valent cations and Mg^{2+} have significantly lower binding constants[71,72,73,74]. The divalent cation concentration $\bar{c}_{++}$ in the bulk medium was varied between $10^{-3} - 10^{-4} M$, a region near the experimental critical calcium concentration to trigger fusion of lipid vesicles[3,6]. Concetration of monovalent ions was held constant at $10^{-1} M$. The dielectric permittivities of the electrolyte solution (ε_s) and PEG (ε_p) were set to 78 and 20, respectively[50,51]. The sizes of monomers, water, and univalent ions were all set to be identical, $3\times10^{-10} m$. The Flory interaction parameter for PEG was set to $v \equiv 1 - 2\chi \approx 0.05$ [76,92] and the degree of polymerization (N) was fixed to 30. The radius of gyration of the polymer was estimated from the relationship: $R_G \approx aN^{\lambda}$, λ being a model-dependent coefficient ($\lambda = 1/2$ for ideal chains, $\lambda = 3/5$ for self-avoiding chains). *MD* simulations of PEG yield[83] $\lambda \approx 0.58$. Next, we examine the effect of different parameters on physical properties.

A) *Interfacial polymer exclusion*

Exclusion of hydrophilic, non-adsorbing polymers (e.g. PEG or dextran) has been experimentally observed[93]. Detection of strong polymer-induced adhesion forces between two opposing membranes has suggested an even more intense polymer exclusion from the lumen mainly due to steric expulsion of polymer chains[94,95,96,97,98]. As we shall discuss later, polymer depletion at mid plane generates osmotic forces, therefore the knowledge of polymer distribution yields useful information on mutual bilayers interactions.

Figure 9 confirms that our model is able to reproduce the above observations. Our results suggest a new mechanism for polymer exclusion based on salting-out effects.

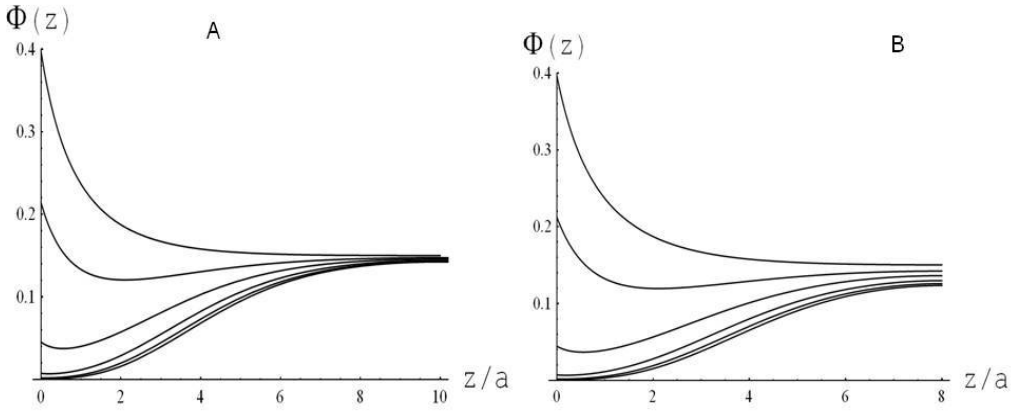

Fig. 9 A.) Polymer concentration profile (volume fraction) inside the gap calculated for different membrane surface charge densities. The membrane surface has been assumed to be moderately attractive for polymer chains (0.5 *kT* per lipid molecule). From the top to the bottom: 0%, 20%, 40%, 60%, 80%, 100% of the maximum charge density (one net charge)/(lipid). The dimensionless intermembrane distance is *D/a=20*. B.) Intermembrane distance *D/a=16*.

Numerical results show even in the presence of weak polymer-surface adhesion, the greater electrolyte concentration generated by the membrane charges deforms the polymer profile. The depletion zone is not localized at the surface (where, conversely, a small polymer enrichment due to non-specific forces is likely to occur), but extends further toward the centre of the gap. Comparison of Figs. 9A and 9B shows the

sensitivity of polymer exclusion in the inter-membrane distance. This dramatic effect depends on the connectivity-related decrease of the polymer mixing entropy that favours phase separation. Numerical results from the analytical model (data not reported) evidence a stronger ion-induced polymer depletion in the case of either long polymers or lower temperatures. Our MD simulations confirm these conjectures. Figures 5a and 5b show the distributions of two polymer chains of different length. Longer polymer chains are more depleted from the inter-membrane space.

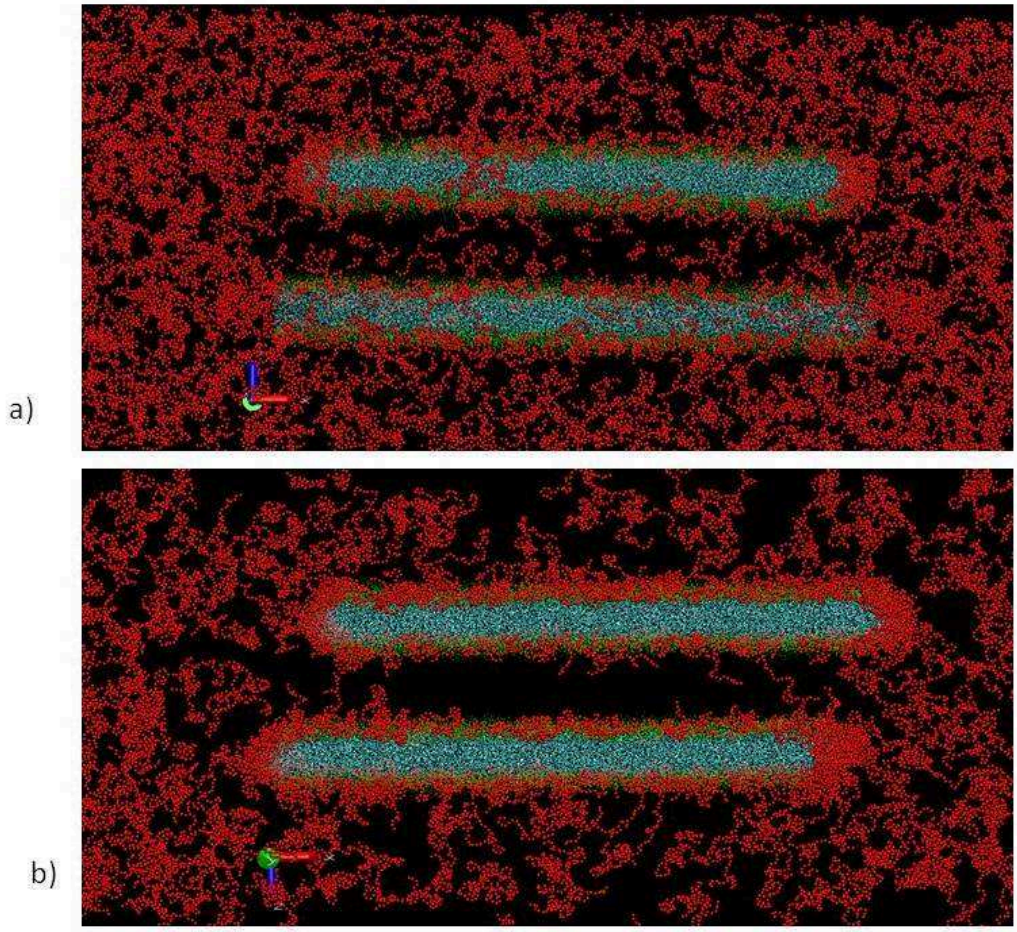

Fig. 10 POPG membranes (light blue) in the presence of 10% of polymer chains made up by 9 beads (red) after 1μs of simulation. b) POPG membranes (light blue) in presence of 10% of polymer chains consisting of 37 beads (red) after 1 μs of simulation. In both systems (a and b) the intermembrane distance is three times the gyration radius of the polymer.

To further explore electrolyte-induced exclusion of neutral polymers, we simulated membranes at different distances. The main results are summarized in Fig. 11

which shows the polymer (PEG) concentration profile $\Phi(z)$ inside a membrane gap as a function of the intermembrane distance for different surfaces.

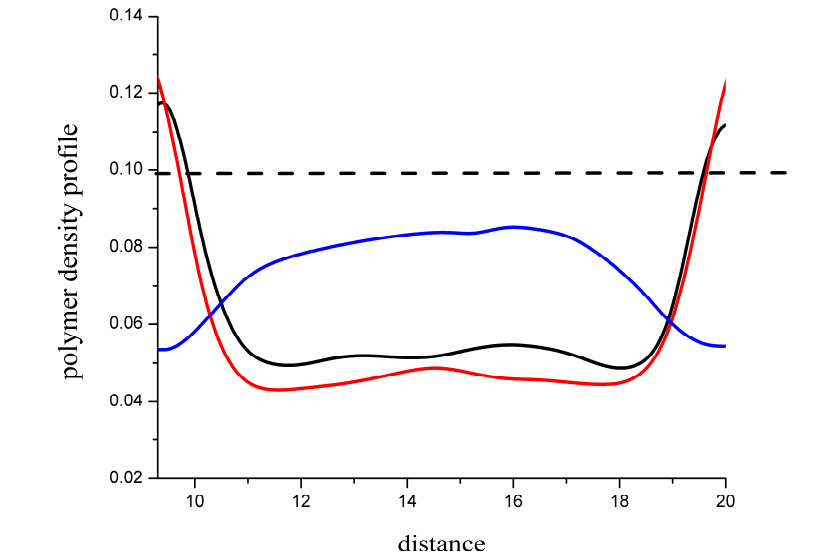

Fig. 11 Polymer (PEG) concentration profile $\Phi(z)$ (volume fraction) inside the gap as a function of the intermembrane distance *D (As)* calculated for different membrane surfaces. The horizontal black dashed line is the average polymer concentration in the bulk. The vertical dotted line identifies the midplane between the membranes. Blue line: polymer density profile in the case of neutral DPPC surfaces. Black line: polymer density profile in the case of negatively charged POPG membranes partially neutralized (75%) by calcium ions. C) Red line: smaller (54%) surface charge neutralization.

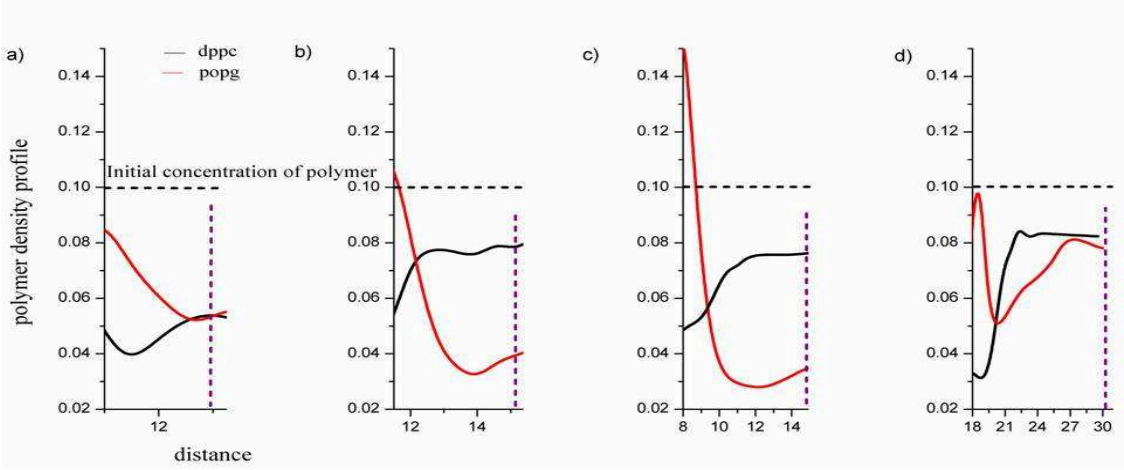

Fig. 12 The polymer (PEG) concentration profile $\Phi(z)$ (volume fraction) inside a membrane gap as a function of the distance from the membrane. The dashed line is the average polymer concentration in the medium. The vertical dashed line represents the mid-plane between the membranes. Black: the density profile of the polymer between neutral membranes of DPPC. Red: the density profile of the polymer between negatively charged membranes of POPG. Both systems contain salt (0.1 M), calcium ions (0.01

M) and polymer (10%). From left to right, we report the density profiles of the polymer between membranes at different distance (a)1 fold, b) 2 fold c) 4 and d) 7 n-folds the gyration radius of the polymer.

PEG concentration decreases inside the intermembrane space for charged systems. As Fig. 12 shows, depletion persists at long distances. When a neutral surface (DPPC) is used, the depletion effect vanishes except for entropic effects at distances ~R_G.

B) *Ion condensation*

As above, we calculated the local electrolyte concentration inside the gap. The results are shown in Fig. 13 where we report the total electrolyte concentration (positive and negative ions) as a function of the distance z from the walls (again, we report only the right half-gap). It is worth noticing that the polymer exclusion described in Fig. 9 determines the observed small electrolyte enrichment near the charged walls as shown in Fig.13.

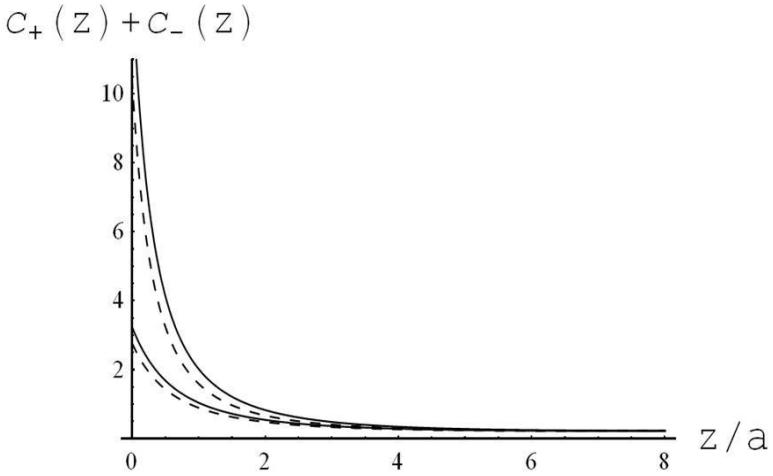

Fig. 13 The total ion concentration profile inside the membrane gap calculated in the absence (dashed lines) and in the presence (full lines) of polymer. The intermembrane distance was set to *D/a=16*., The fraction of charged lipid was 80% (upper curves) and 40% (lower curves). These conclusions are fully confirmed by MD simulations shown in Fig. 14.

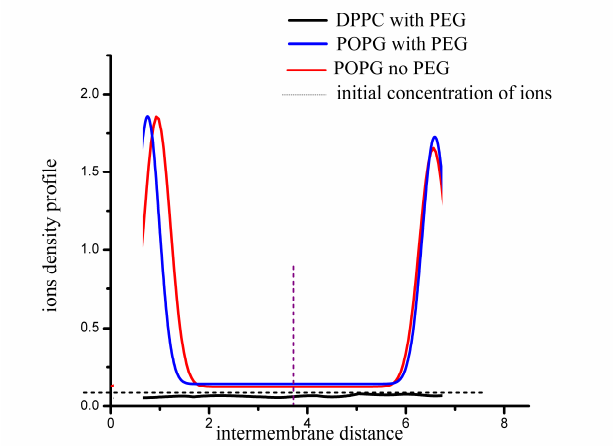

Fig. 14 MD profile of the total ion concentration (7241 sodium ions, 3073 chlorine ions) inside the membrane gap calculated in the absence (red line) and in the presence (blue line) of polymer in the systems of POPG lipids after 1μs. The black line shows the ion density profile in the systems with DPPC in presence of PEG. The black dashed line is the average ion concentration in the medium. The violet dashed line represents the mid distance between the two membranes.

A few points are worth mentioning: a) Both analytical and *MD* computations show that the decays of polymer and electrolyte concentration profiles are very different (Figs. 9-12 and 13-14), the ion excess being localized in a narrow region near the interface. b) The electrolyte-induced polymer exclusion from charged surfaces is particularly evident when moderate attractive polymer-surface interactions are introduced (polymer-membrane van der Waals and polarization forces are stronger than water-membrane forces), while in the case of strong polymer-surface incompatibility, salting-out effects are masked to a large extent because polymer has been already depleted from the surface (data not shown). c) The electrolyte-induced polymer exclusion persists even at large inter-membrane distances. This effect cannot be predicted by Asakura-Oosawa like theories[70] where the polymer concentration suddenly falls when the interplates distance is shorter than the chains gyration radius, while it remains constant at larger distances (the smoother decay found in the literature is due to the finite radius of the interacting particles here simulated as infinite plates).

C) *Intermembrane forces and distances.*

Membrane charges have different effects on the inter-membrane forces. The most obvious one is the electrostatic repulsion between them. Other effects are more subtle. Ion-induced polymer exclusion from charged membranes modifies the decay rate of the osmotic forces as they become more long-ranged than predicted by theories based on steric exclusion. These effects are shown in Fig. 15 where we report the electrostatics forces (dashed lines) and the depletion forces (dotted lines) as against the charged plates distance *D/a*. When all the polymer chains have been excluded from the gap (short plates distance) the depletion forces reach a plateau (data not shown). On the contrary, at large plates distances, the salt-induced polymer exclusion is weak because of a smaller ion density within the gap, making the decay of the osmotic forces smoother. It is worth mentioning that: a) the enhancement of depletion forces with the plates' surface charge, b) forces are sensitive to the conditions set at the polymer-membrane surface. In the case of sticky surfaces, depletion effects are smaller, a result already observed in simpler systems[99].

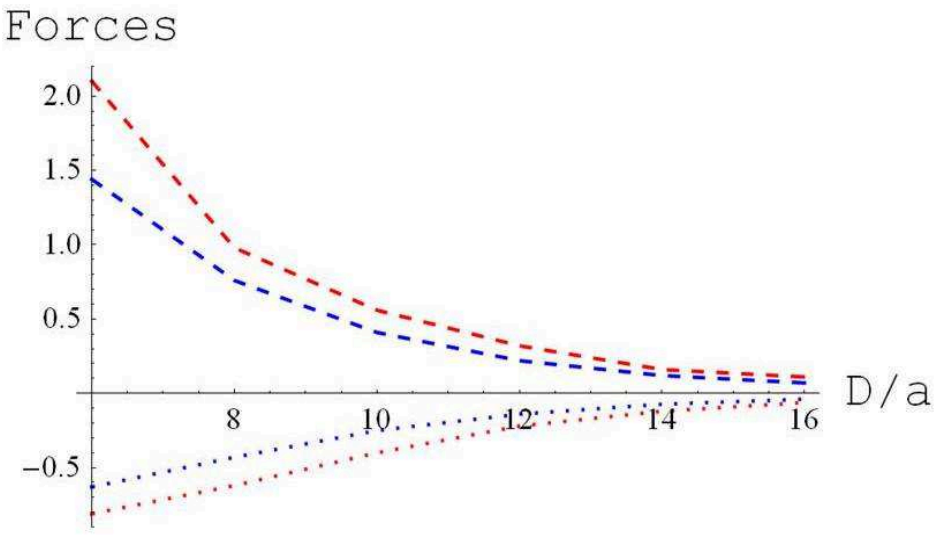

Fig. 15 Inter-membrane forces ($\times 10^5 N \cdot m^{-2}$) as a function of the dimensionless relative distance *D/a* at two different surface charges (40% (blue) and 100% (red). The bulk polymer volume fraction is 0.15. The dashed lines show the electrostatic component and dotted lines the depletion forces. As the surface charge density increases, the total interaction (the sum of the two components) between the charged membranes remains basically unmodified.

Let us turn to the electrostatic forces. At physiological salt concentrations, the decay of Coulomb repulsion is faster than that of depletion forces. For small *D/a*, most chains are excluded from the gap and depletion forces attain their maximum values. On the other hand, when the chains are excluded from the gap, the local higher dielectric constant generates an electrolyte flux from the bulk to the gap and modifies the strength and decay of polymer-mediated Coulomb forces.

Similar behaviour is observed in our *MD* calculations where an extensive polymer depletion at mid plane $z=D/2$ (see Fig. 12) is accompanied by a slight but detectable increase of the ion concentration (data not shown). Unfortunately, noise is high because one is sampling a relatively small group of particles at mid plane, so any further attempt to quantify the strength of electrostatic and depletion forces obtained through *MD* simulation is left to future studies.

Several experimental studies have determined the strength and decay of the inter-membrane forces in the presence of polymers. Most of them use surface force apparatus or micropipette aspiration techniques[73]. Most of these studies deal with neutral vesicles, and only a few address the interaction between charged vesicles[100,101]. Other authors have investigated the collective behaviour of interacting spheres suspended in a polymer solution[102], by scattering techniques. Lastly, measurements on charged rigid spheres have also been performed by techniques such as total internal reflection microscopy[103,104,105]. Our theoretical results are in qualitative agreement with the experimental data that show a subtle interplay of osmotic and electrostatic forces leading to decay lengths of the osmotic forces much larger than expected.

D) Ion Binding to Charged Membranes

The behaviour of multi-valent cations that may neutralize the membrane charges by forming tight bonds with anionic lipid head groups is very different from that of the usual electrolytes. A list of related phenomena is as follows:

Concentration of bound ions. A first result concerns the concentration of adsorbed multi-valent cations. This is a key parameter to understand the adhesion/fusion

mechanism. Indeed, adsorbed cations (mainly Ca^{2+} and Mg^{2+}) may form either *trans* complexes between negative lipids belonging to the same membrane, or *cis* complexes between lipids belonging to opposite membranes. Obviously, *cis* complexes appear only when the membrane distance is of order of the ion diameter, otherwise only *trans* complexes appear. *Cis* bonds are believed to be tighter than the *trans* ones[106,107]. A likely mechanisms making PEG so efficient in inducing membrane adhesion/fusion could be related to the increased concentration of bound divalent cations (*trans* complexes). When thermally-induced fluctuations of the inter-membrane distance bring apposed membranes at close contact, the sudden switch from *trans* to *cis*-complexes stabilizes a focal contact which may act as a nucleation site for further expansion of the adhesion region[31,108].

We used equation (32) to calculate the fraction θ of neutralized sites as a function of the bulk divalent concentration both in the absence and presence of constant polymer volume fraction,

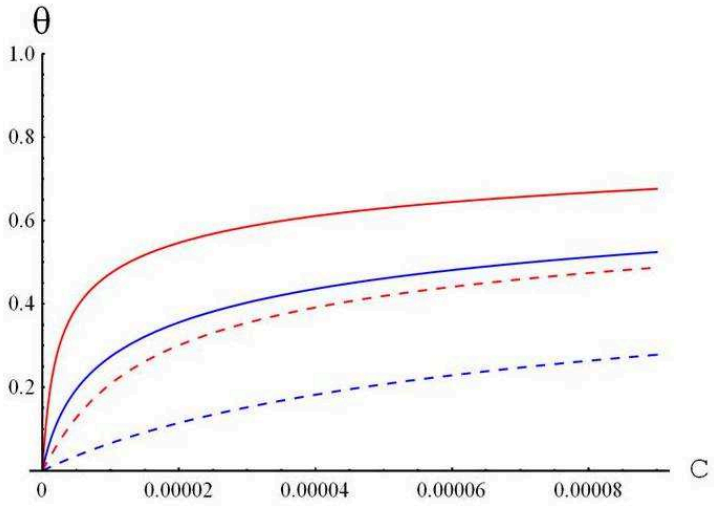

Fig. 16 The fraction of neutralized charged sites θ versus the bulk concentration *C* of divalent cations dissolved in a *0.1 M* electrolyte solution (monovalent ions). Full lines refer to a polymer containing water solution ($\overline{\Phi} = 0.15$), the (charged lipids)/(total lipids) ratio was 0.4 (blue) and 1.0 (red). For comparison we report also the corresponding curves calculated without polymer addition ($\overline{\Phi} = 0.0$, dashed curves).

Curves arise from a balance between several effects. Polymer addition makes the bulk solvent less polar, forcing all kinds of ions inside the gap, causing the amount of

bound cations to increase. This term behaves as $e^{+|const|z_{\mp}^2}$, thus it is very sensitive to the charge of the adsorbed ion. At low coverage ($\theta << 1$) collective effects arising from surrounding charged headgroups are strong and largely contribute to the ion binding. On raising surface neutralization by bound ions ($\theta \approx 1$), the only relevant interaction occurs between an adsorbing ion and an apposed lipid head. This implies a smaller effective binding constant. The net result is a rapid initial growth of the binding followed by a smooth increase of the bound ions fraction (anti-cooperative effect).

These results are confirmed by the *MD* simulation data summarized in Fig.17. The increase of polymer-induced fraction of bound divalent ions, especially at short intermembrane distances, is clearly visible. This is very different from the effect of mono-valent ions that show only a modest enhancement, Fig. 14. This comparison highlights the specificity effects related to the sensitivity of the solvation energy on the solute charge density. Unfortunately, the equilibration times are extremely long because the calcium ions bound to oppositely charged lamellas diffuse through hopping mechanism over the membrane plane, a finding already observed in experimental studies of lamellar bunches[88,89]. Furthermore, the presence of PEG further damps the ion diffusion rate, as found in real systems[109]. These drawbacks introduce a large error in our *MD* data.

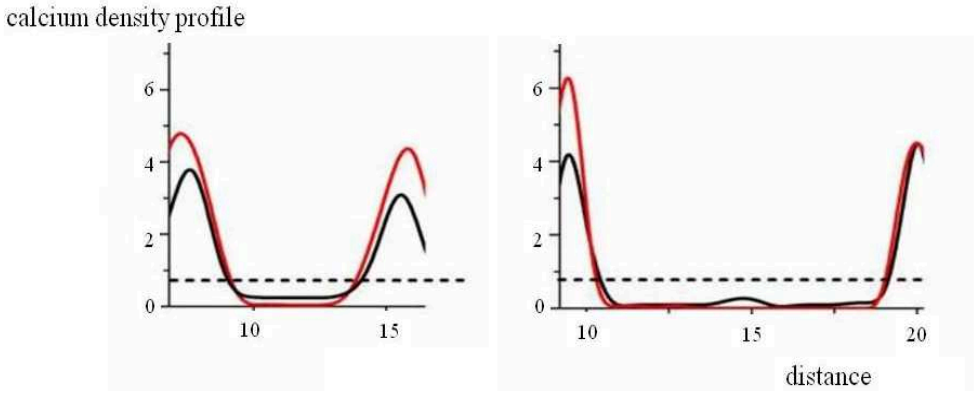

Fig. 17 The density profile between charged membranes of an absorbable divalent cation (500 calcium ions) dissolved in a *0.1 M* electrolyte solution (7241 sodium ions, 3073 chlorine ions) calculated at two different inter-membrane distances. Red lines refer to a polymer-containing water solution. For comparison we report also the corresponding curves calculated without polymer addition (black line); dashed line is the average ion concentration in the medium.

Qualitatively, our results confirm earlier suggestions on the polymer enhancement of bound ion concentration[110]. This effect has been postulated by several authors to explain the synergistic effect of ions and polymers on association phenomena (see, e.g., ref. 111), but, unfortunately, no direct, unambiguous measurements exist to our knowledge.

Role of Ion Binding on the Polymer Profile. Ion adsorption neutralizes the surface charges and reduces polymer expulsion from the inter-membrane gap. This phenomenon is clearly shown in Fig.18 where we report the polymer profile within a charged gap calculated at increasing surface charge neutralization.

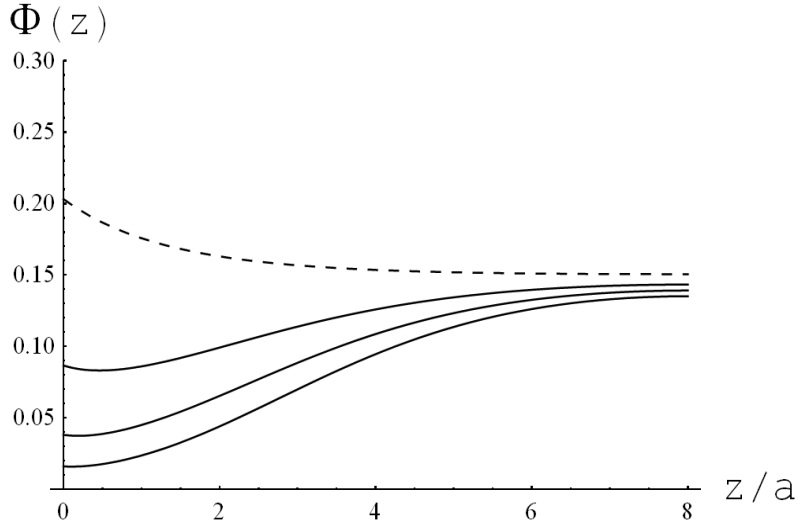

Fig. 18 The effect of surface ion binding on the polymer profile within the intermembrane gap: The dashed line is the polymer profile in the absence of surface charges. Other lines have been calculated for different neutralization degree induced by the surface binding of divalent cations: from the bottom to the top: 0.0 M, $10^{-5}M$, $10^{-4}M$. Charge neutralization was calculated from the data of Fig.16. The (charged lipids)/(total lipids) ratio was 0.2, while the polymer volume fraction in the bulk was $\overline{\Phi} = 0.15$.

The above results highlight the dramatic difference between the different kinds of ions in inducing polymer depletion: ions that concentrate themselves near the charged surface but do not bind (defined as bulk ions) are very effective in inducing polymer depletion. On the other hand, bound ions (e.g. divalent cations) have the opposite effect because they reduce the Coulomb interactions that provide the driving force for polymer depletion. These conjectures were confirmed by our MD simulations: negatively charged POPG membranes begin to behave like the neutral DPPC ones upon

full charge neutralization (see, e.g., Fig.11).

Role of Ion Binding on the Inter-membrane Forces. The neutralization of surface charges has complex effects on the inter-membrane forces. The most trivial one is the reduction of the electrostatic repulsion between opposing membranes[112]. Our model shows, however, that polymer chains remain significantly excluded from the lumen region, even at rather large D, because of the higher ion concentration (see point A). Surface charge neutralization induces a polymer backflow inside the gap as shown in Fig.13 ($D>R_G$). As a consequence, depletion forces decrease because of the levelling polymer concentration in the gap and in the external reservoir. At the same time, surface charge neutralization pushes the electrolytes toward the bulk, relieving the repulsive excess osmotic forces of the ions. Therefore, the response of a membrane-polymer system to surface charges neutralization depends on a subtle balance between decreased depletion attraction and polymer-modulated electrostatic repulsion, Fig. 16.

Such homeostatic behaviour evidences the opposite response of osmotic and coulomb forces to the surface charge density of interacting bodies. It could explain why non-adsorbing uncharged polymers are so effective in inducing adhesion of both neutral and charged colloidal particles[6].

We have derived a simple analytical model to describe the interaction between two planar charged membranes embedded in a polymer-containing electrolyte solution. The inter-membrane gap and bulk solution may interchange matter in order to attain minimum energy conditions. We considered uncharged polymers with monomers that have a lower dielectric permittivity than the solvent molecules. The electrolyte solution mimics a physiological fluid: it contains ~0.1 M mono-valent ions together with a small number of divalent cations that are able to form tight bonds with the charged lipid headgroups. We derived an analytical model that allowed us calculate the polymer and electrolyte profiles, the fraction of bound ions, the inter-membrane forces as a function of the surface charge density and the fluid composition and solvation energies of ions.

The validity of our analytical results was confirmed by extensive coarse-grained

MD simulations. It should be noticed, however, that simulations and the analytical model describe slightly different systems: While the analytical model assumes ions and polymers partitioned between the inter-membrane space and an infinite external reservoir, simulations have a finite reservoir. This unavoidable limitation introduces some differences in entropic forces. As a consequence, the ions' migration from the bulk to the inter-membrane space is underestimated because the finite external reservoir is depleted from the adsorbed/bound ions within the gap. The same reasoning applies to polymer chains. The magnitude of this finite size effect depends on concentration and it is greater in dilute solutions. In principle, the finite size effect could be estimated by varying the reservoir size V and extrapolating the simulation results to $V \to \infty$. This implies that both polymer depletion and salt enrichment inside the gap calculated by *MD* simulations should be even more evident than reported here (curves in Figs.14 and 17 should lie over the dashed line representing the bulk ion concentration, in agreement with the analytical findings).

6. CATCHING THE FUSION EVENT

6.1 System evolution

6.1.1 Contact

As previously discussed, membrane fusion lies at the heart of important biological processes. In vivo, membrane fusion is tightly regulated by proteins. The basic mechanism, however, is primarily determined by the physics of lipid-lipid interactions[113].

We performed molecular dynamics simulations to investigate the molecular details of the process of fusion for giant vesicles.

Besides van der Waal's attractive force, there are hydration, electrostatic, and steric forces that produce strong repulsive force adequate enough to prevent the close contact of the approaching membranes[114].

Lowering of the number of water binding sites or charge on the membranes decreases the lipid bilayer repulsion, which facilitates close contact of the membranes[115]. **Different fusogenic agents can diminish this hydration repulsion[116].** An estimated pressure is required to mix or merge the outer leaflet of contacting membranes[117], which is very high.

After the releasing of constraints, the two opposite fluctuating membranes can finally approach to each other.

In the following table 2 we report the average distance between the two charged opposite bilayers in presence or absence of polymer calculated after 500ns of simulation.

System\ average value	Av. Distance	Min. distance
POPG no PEG	8.58	1.63
POPG with PEG (10%)	7.96	0.138

Table 2 polymer effect on the equilibrium distance between two opposite charged bilayers after 500ns of simulation.

Lentz and co-workers[116] reports the variation of the fusion rate with the distance (measured by X-Ray diffraction and externally tuned by polymer-induced depletion

forces). Recent measurements by combined micromanipulation and fluorescence techniques show similar behaviour too[118]. The lower intermembrane distance induced by the presence of polymer suggests in agreement to experimental results[107,110] and theoretical predictions (ref) a higher fusion rate[31].

To minimize the work required for lipid merger, initial contact proceeds is expected to through small, local point of contact. This leads to the participation of minimum number of lipid molecules during formation of the fusion intermediates. Thus, merging of lipid membranes becomes a very site-restricted process, acting in some cases within a very small area[119].

Thermally excited fluctuations may give a rise to a local protrusion connecting the two membranes[108].

When we compare the systems d, g, **the main outcome concerns the evident tendency of charged membranes to interact, conversely to the neutral membranes** (Fig. 19). The equilibration of the system (e) with 30% of polymer is very slow, so it will not be taken in account and discussed in the present thesis.

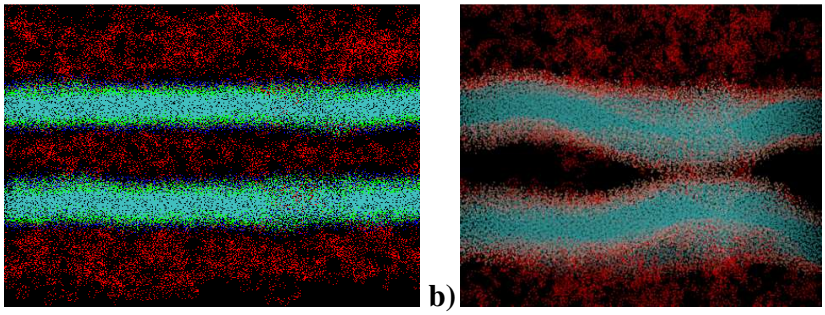

Fig. 19 a) DPPC membranes in presence of 10% of PEG (red beads) b) POPG membranes in presence of 10% of PEG (red beads).

As previously discussed in section 5, the higher tendency of POPG membranes to interact is probably related to the higher concentration of bridges-forming divalent cations in the intermembrane space and the reduction of the electrostatic repulsion.

From the other hand, as experimentally shown, a decrease of fluctuation amplitude is found as the solvent viscosity increases[120]. This suggests a lower probability to have active fluctuations to form an initial contact site because a higher viscosity induced by the increased concentration of PEG in the medium.

We report in table 3 the mean square displacements (msd) of the bilayer' atoms from the average positions along the main axes (fig. 19). At the increased concentration of PEG corresponds a fluctuations decay.

System / msd	Axes z	Axes y	Axes x
POPG no PEG	**0.009**	0.21	0.24
POPG 10% of PEG	**0.0017**	0.19	0.21
DPPC 10% of PEG	**0.0002**	0.28	0.29

Table 3 msd of the POPG and DPPC atoms in presence in presence of different concentrations of polymer.

Apparentely charged membranes in absence of polymer have more chance to enter in contact.

The transient adhesion site is stabilized by short range adhesion forces and it is destabilized by repulsion and elastic deformation energy[31].

The fusion process in our case is triggered by a fluctuation of the two opposite bilayers which results in some head groups merging to form a contact site that appears stabilized by positively charged ions (Na^+ and Ca^{2+}) as showed in Fig. 20.

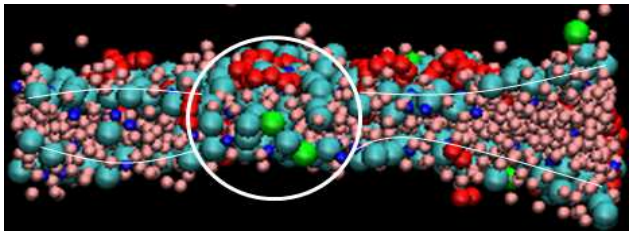

Fig -20 spot of the contact site where calcium ions (green) promote the cis interactions between headgroups (cyan) belonging to opposite bilayers.

In the three different tests, repeated at three different initial velocities, the contact site was persistent in presence of polymer, where instead, in absence of polymer, charged membranes where adhering only in one of the three trials, and the dimension of the adhesion site was much smaller ($24nm^2$) compared to the contact site formed in presence of polymer ($36nm^2$). The concentration of calcium ions forming cis bridges between the two opposite membranes in presence of polymer was the 8% of the total amount of head-

groups involved in the contact, 4% more of the total amount of calcium present in the adhesion site in absence of polymer.

If we look at the distribution of the calcium ions in the intermembrane space in presence or absence of polymer versus time, from preliminary assets, a coherent accumulation of calcium ions, close to the site destined to become a contact, is evidenced (fig.21).

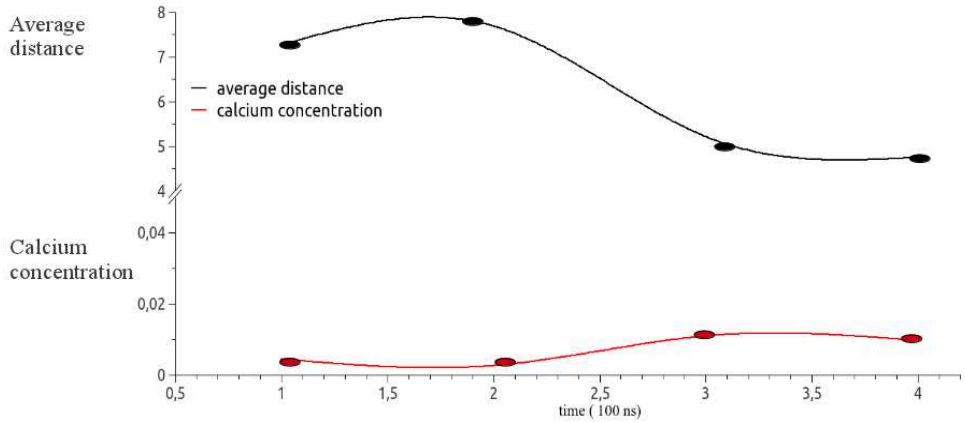

Fig.21 Concentration profile of calcium ions vs time (red line) in a potential contact site between two approaching charged membranes (black line).

Above of a critical radius of the contact site, adhesion forces prevail, enabling the contact site to expand until complete membrane-substrate adhesion is attained. These results confirm the model of fusion developed in Chapter 1[31].

6.1.2. Merging

After the formation of an initial contact site between opposite charged membranes the pore, generated to promote the exchange of species in or out the intermembrane space, was closed. In this way, we wished to catch the fusion event.

After the close contact of the two approaching membranes or lipid bilayers, a temporary disorder of the bilayer lipids in the contact region is required for vesicular merging. According to a school of thought[121], **during the merging of lipids,**

considerable amount of lipids undergo a transition from lamellar bilayer phase (L) to inverted hexagonal phase (HII) (Fig. 21)[122] **at the contact site**. **It has been proposed that, the transition from L → HII is essential for the successful mixing of the outer bilayer of lipids to promote fusion.** There are a number of molecules like surfactants[123], solvents[124,] and metabolites[125] which can influence the L → HII phase transition and thereby have the propensity to act as fusogens.

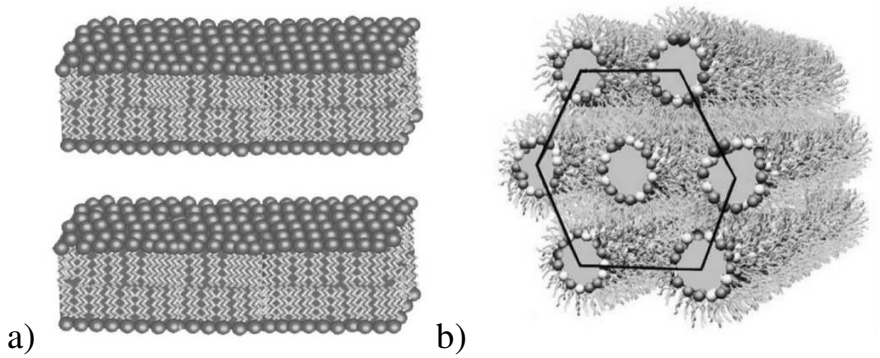

Fig- 21 Different phases of lipid: (a) lamellar (L) phase and (b) inverted hexagonal (HII) phase.

Another factor that facilitates the merging of the lipids and thus promotes fusion is accumulation of defects or perturbations or fluctuations in the contact region. Defects can be introduced either by external agents like fusogens, or by alteration of some physical parameters. **It is well known that temperature[41], membrane curvature[126] can stress the membranes.**

We increased the temperature from 300k to 400k to check the strength and to accelerate the propagation of the site. This resulted in a linear growth, rather than circular, because the periodic boundary conditions and the high temperature that favored the stabilization of inverted hexagonal (HII) phase (Fig.22).

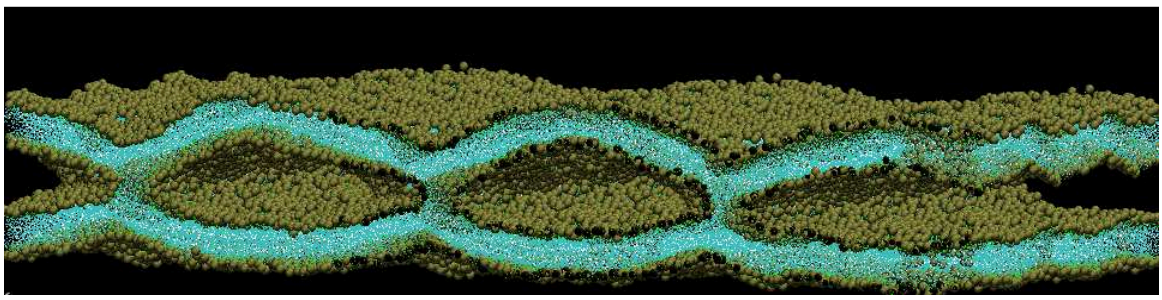

Fig. 22 Opposite charged membranes (cyan) in contact formed inverted hexagonal (HII) phase.

Along the linear contact site, we were able to observe some spots (Fig. 23) where lipid heads move away leaving space to the deeper and stronger interaction between lipid tails belonging to opposite layers: we had hemifusion!

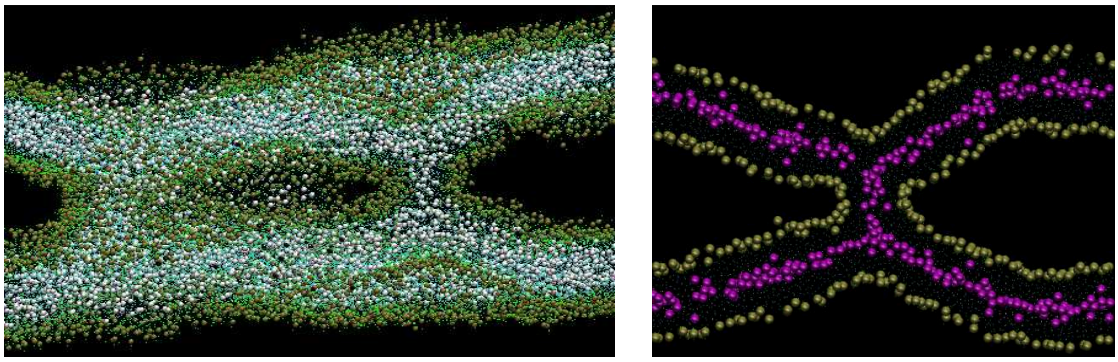

Fig. 23 a) POPG membranes merged: white beads represent lipid tails and green beads represent the headgroups. b) Thin section (1nm) of the deepest contact spot. In violet, the end terms of the lipid tails and in green the headgroups.

Typically after the hemifused state, a small fusion pore appears[127]. Once this happens the bilayer ruptures, completing the fusion process. As predicted theoretically[19], the high energy of the stalk intermediate is solved by tilting of the tails, avoiding empty voids.

In order to move on, we needed to restore the pore, far from the contact region, to liberate the trapped water and ions. In addition, we modified the parameterization increasing the favorable interactions between the tails beads to promote the complete fusion trough the formation of a pore [128].

Because the stability of the simulated system for long time of simulations (microseconds), we realized at this point about the irreversibility of the linear propagation of the fused site. The stress was not enough to induce the membrane rupture in the contact region.

A new set of simulations will be performed at 300k. In this way, we expect to avoid the formation of inverse phases and, keeping the free pore since the formation of the first contact, we wish to observe a circular growth of the site.

In any case, we reached an important outcome. Until now, the only try to simulate the fusion process has involved small vesicles with a high local membrane stress, far from the average biological sizes. In addition, to promote the interaction between

opposite bilayers, in most of the cases are taken in account the well-Known fusogenic proteins. For the first time, we are considering instead the combined effect of polymer and calcium ions on the spontaneous merging and fusion between soft objects of infinite size.

7. Resume and CONCLUSION

Our computational results show:

- ✓ The evident decrease of PEG concentration between opposite charged membranes also when the intermembrane distance is bigger than the gyration radius of the polymer.

- ✓ The intermembrane distance between two charged membranes is decreased in presence of polymer. Shorter distance enhances the fusion rate.

- ✓ The concentration of cations in the membrane region in presence of PEG was higher than in the system without PEG.

- ✓ We observed from the initial steps that the membranes in presence of PEG had a higher trend to form initial contact sites despite smaller fluctuation amplitudes.

- ✓ A higher concentration of calcium ions localized at level of the adhesion site stabilized the merging of head-groups belonging to opposite bilayers.

As theoretically predicted in of my thesis the polymer effect is threefold:

a) Enhanced membrane adhesion because of a higher concentration of bridges-forming divalent cations.
b) Enhanced adhesion because of polymer-induced osmotic forces.
c) Reduction of the electrostatic repulsion.

It is worth noting that the unbalance of the electrostatic pressure upon polymer addition is not merely due to a decrease of the solvent dielectric permittivity, rather it depends on polymer salting-out effects favoured by the charged surfaces.

A cascade of phenomena depends on the polymer-enhanced attraction between lipid membranes. Stronger attraction means a greater number of weakly associated vesicles and therefore a higher inter-vesicular fusion rate.

Furthermore, the polymer-enhanced fraction of adsorbed divalent cations at the membrane surface (due to salting-out property of uncharged polymers) provides a pool of bridges-forming cations required to connect apposed membranes locally brought at close contact by thermally excited fluctuations.

The positive combination of these factors may explain why hydrophilic polymers are so effective in triggering adhesion and fusion of lipid vesicles even in the presence of unfavourable strong coulomb repulsion.

ACKNOWLEDGEMENT

I want to express my sincere gratitude to my supervisor, the professor A. Raudino. His wide expertise and his strong ability of logical thinking have provided the basis for the present thesis, teaching me to perseverate in the research of the best way to face and solve the problems.

In addition, I want to thank the professor Mikko Kartunnen, that during my visit to his research group in London (CA), assisted me in the use of the computational approach with precious suggestions.

Finally, I would like to thank the professor S.J. Marrink that gave me the chance to visit his computational group in Groningen (NL) and learn more about the Martini forcefield, in particular thanks to the helpful collaboration with the PhD student Djurre De Jong.

We thank CINECA (Italy), SharcNet (CANADA) and Sara (The Netherlands) for providing the computational resources used in this project.

APPENDIX A

Consider a constrained functional H defined as

$$H = E_{TOT} - \int_0^{D/2} (\mu_{\bar{\Phi}} \tau^2(z) + \sum_i \mu_{\bar{c}_i} c_i(z) + \mu_{\bar{\psi}} \psi(z)) dz \qquad (1A)$$

where μ_j s are undetermined Lagrange multipliers and the total free energy E_{TOT} is given by (12). Minimization of a generic functional G defined as:

$$G \equiv f_1(y_1(z)|_{z=D_1}, y_2(z)|_{z=D_1}, ..., y_n(z)|_{z=D_1}) +$$

$$f_2(y_1(z)|_{z=D_2}, y_2(z)|_{z=D_2}, ..., y_n(z)|_{z=D_2}) +$$

$$\int_{D_1}^{D_2} F[y_1(z), y_2(z), ..., y_n(z), \partial y_1(z)/\partial z, \partial y_2(z)/\partial z, ..., \partial y_n(z)/\partial z] dz \qquad (2A)$$

yields n Euler-Lagrange equations

$$\frac{\partial F}{\partial y_j(z)} - \frac{\partial}{\partial z} \frac{\partial F}{\partial (\partial y_j(z)/\partial z)} = 0 \qquad (3A)$$

together with $2n$ boundary conditions

$$\left. \frac{\partial f_1}{\partial y_j(z)} \right|_{z=D_1} - \left. \frac{\partial F}{\partial (\partial y_j(z)/\partial z)} \right|_{z=D_1} = 0 \qquad (4Aa)$$

$$\left. \frac{\partial f_2}{\partial y_j(z)} \right|_{z=D_2} - \left. \frac{\partial F}{\partial (\partial y_j(z)/\partial z)} \right|_{z=D_2} = 0 \qquad (4Ab)$$

Our variational functions are $c_i(z)$, $\tau(z)$ and $\psi(z)$, while the domain boundaries are at $D_1 = 0$ and $D_2 = D/2$ (the system is symmetric with respect to the half-plane $z = D/2$).

APPENDIX B

When the distance *D* between the two opposing surfaces is much larger than R_G ($\approx N^{3/5}$) of a single polymer coil, the polymer concentration in the central region of the membrane gap is similar to that in the bulk. Hence, when $\varsigma \approx D/2a$ >>1 we can write the scaled polymer concentration as $\tau^* = 1 - \xi\eta(\varsigma)$ with $\xi << 1$. The same reasoning applies to the potential ψ_o^* that must be very small too, of order ξ. Inserting $\tau^* = 1 - \xi\eta(\varsigma)$ into (20a,b) and neglecting higher order terms in ξ^2, we get

$$\frac{\partial^2\eta}{\partial\varsigma^2} - 2A\eta = AG_1(\psi_o^*,1) \qquad (1Ba)$$

$$\frac{\partial^2\psi_o^*}{\partial\varsigma^2} = \bar{\kappa}^2 a^2 \sinh(\psi_o^*) \qquad (1Bb)$$

where

$$G_1(\psi_o^*,1) = \lim_{\tau^*\to 1} G_1(\psi_o^*,\tau^*) \equiv (\varepsilon_p - \varepsilon_s)\left(\frac{akT}{8\pi e^2}\left(\frac{\partial\psi_o^*}{\partial\varsigma}\right)^2 + 2\frac{B\bar{c}_M}{\bar{\varepsilon}^2}(\cosh(\psi_o^*)-1)\right)$$

and $A \equiv 6(1-2\chi)\bar{\Phi}$. In the case of a single charged surface in a medium of dielectric permittivity $\bar{\varepsilon}$, (1Bb) has an analytical solution[19]. When D/a is large, we may use the so-called weak overlap approximation, where $\psi(z)$ stems from the potentials of two isolated surfaces:

$$\psi_{eff}^*(\varsigma) = \psi_o^*(\varsigma) + \psi_o^*(D/a - \varsigma) \qquad (2Ba)$$

where the isolated membrane potential is given as

$$\psi_o^*(\varsigma) = 2\log\frac{1+\Gamma e^{-\bar{\kappa}a\varsigma}}{1-\Gamma e^{-\bar{\kappa}a\varsigma}} \qquad (2Bb)$$

$\Gamma \equiv tgh(\frac{1}{4}\psi_o^*\big|_{\varsigma=0}) < 1$. Equation (2Ba) automatically satisfies the boundary condition (16a) and the second boundary condition is given by (18b). Because of the large ion concentration near the charged interfaces, most of the chains are expelled from the interface (this was confirmed by MD simulations). Due to this, the interfacial dielectric constant approaches that of the solvent, $\varepsilon(\tau^*\big|_{\varsigma=0}) \approx \varepsilon_s$. Using this result, together with the analytical expression for the potential (2Ba,b) we can use (18b) to derive $\varepsilon_s\bar{\kappa}a(1-\Gamma^2)^{-1} = -\pi(e^2/akT)(a/b)^2 X$. This enables us to relate the surface potential $\psi_o^*\big|_{\varsigma=0}$ and the surface density $\sigma \equiv eX/b^2$ as

$$\Gamma \equiv tgh(\tfrac{1}{4}\psi_o^*\big|_{\varsigma=0}) = \frac{1}{\alpha}\left[1-\left(1+\alpha^2\right)^{1/2}\right] \qquad (3B)$$

where $\alpha \equiv 2\pi e^2 X / \varepsilon_s \bar{\kappa} b^2 kT$. Therefore, the function $G_1(\psi_o^*,1)$ contained in (1Ba) becomes: $G_1(\psi_o^*,1) \approx const \cdot (e^{-2\bar{\kappa}a\varsigma} + e^{-2\bar{\kappa}a(D/2a-\varsigma)})$ + *faster decaying terms*. Inserting this into (1Ba) and introducing the scaled distance $\varsigma^* = D/2a + y$, we find to the leading terms

$$\frac{\partial^2\eta}{\partial y^2} - 2A\eta \approx \Lambda\cosh(\lambda y) \qquad (4B)$$

where $\Lambda \equiv 8\frac{\varepsilon_p - \varepsilon_s}{\bar{\varepsilon}} A\Gamma^2\left(1-\frac{2B}{\bar{\varepsilon}}\right)e^{-\bar{\kappa}D/2}\bar{c}_M$. Since the high interfacial ion concentration expels most of the less polar polymer chains from charged surfaces, we can apply a simpler boundary condition $\eta\big|_{y=\pm D/2a} = 1$. In addition, symmetry imposes the boundary condition $\partial\eta/\partial y\big|_{y=0} = 0$. Solving (4B) and substituting back the original distance *z* and polymer concentration $\Phi(z) = \bar{\Phi}(1-\eta)^2$, we get the simple result reported eq.(20) of the main text.

REFERENCES

1 **J. Rizo and C. Rosenmund**, Nat. Struct. Mol. Biol. **15**, 665 (2008)

2 **S.C**. **Harrison** Nat. Struct. Mol. Biol. **15**, 690 (2008)

3 **J. Zimmerberg and L. V. Chernomordik**, Science, **310**, 1626 (2005)

4 **K. Arnold,** in Handbook of Biological Physics, edited by R. Lipowsky and E. Sackmann (Elsevier, New York), Vol. 1,903 (1995).

5 **B. R. Lentz**. Eur. Biophys. J. **36**, 315 (2007)

6 **D. Needham and D.H. Kim**, Colloids Surf. B, **18**, 183 (2000)

7 **V. A. Bloomfield,** Curr. Opin. Struct. Biol. **6**, 334 (1996)

8 **G. Kleideiter and E. Nordmeier,** Polymer **40**, 4025 (1999)

9 **M. Boncina, J. Rescic, and V. Vlachy,** Biophys. J. **95**, 1285 (2008)

10 **M. Hosek, J. X. Tang,** Phys. Rev. E **69**, 051907 (2004)

11 **D. .J. Needleman, M. A. Ojeda-Lopez, U. Raviv, K. Ewert, J. B. Jones, H. P. Miller, L. Wilson, C. R**. **Safinya,** Phys. Rev. Lett. **93**, 198104 (2004)

12 **A. M. Stephan**, Eur. Polym. J., **42**, 21 (2006)

13 **I. F. Hakem, J. Lal, M. R. Bockstaller,** Macromolecules **37**, 8431 (2004)

14 **F**. **Quina, L. Sepulveda, R. Sartori, E.B. Albuin, C.G. Pino, E.A. Lissi,** Macromolecules, **19**, 990 (1986)

15 **Hatti-Kaul, Rajni**, Aqueous Two-Phase Systems, Methods and Protocols, Humana Press; 1 edition (2000)

16 **J. Schindler, H.G. Nothwang**, Proteomics **6**, 5409 (2006)

17 **A. Kulkarni, C. Zukoski** J Cryst Growth **232**, 156 (2001)

18 **S. Finet, D. Vivares, F. Bonnete´, A. Tardieu,** Meth. Enzym., **368**, 105 (2003)

19 **J.N. Israelachvili**, Intermolecular and Surfaces Forces, Academic Pres, San Diego, (1995)

20 **R.P. Rand and V.A. Parsegian**, Biochim. Biophys. Acta, 988, 351 (1989).

21 **J. Formsnan, C.E: Woodward, B. Jonsson**, Langmuir, 23, 5454 (1997)

22 See, e.g. **D. Leckband**, Curr. Opin. Colloid Interfaces Sci., 6, 498 (2001)

23 See, e.g. **R.F. Bruinsma, A. Behrisch and E. Sackmann**, Phys. Rev. E, 61, 4253 (2000) and references therein.

24 See, e.g., **D.M. Zuckermann and R.F. Bruinsma**, Phys. Rev. E, 57, 964 (1988)

25 **S. Ohki and K. Arnol**, Colloids Surf. B, 18, 83 (2000)

26 **U. Seifert and R. Lipowsky**, Morphology of Vesicles, 1995, Elsevier, Amsterdam

27 See, for instance: (a) **A. Hategan, R. Law, S. Kahn and D.E. Discher**, Biophys. J., 85, 2746 (2003) (b) **V.S. Malinin, P. Frederik and B.R. Lentz**, Biophys. J., 82, 2090 (200)

28 (a) **E. Evans and W. Rawicz**, Phys. Rev. Lett., 64, 2094 (1990); (b) **E. Evans and V. Heinrich**, C.R. Phys., 4, 265 (2003)

29 **W. Helfrich**, Z. Naturforsch., C 28, 693 (1973)

30 a) **I. Bivas and P. Meleard**, Phys. Rev. E, 67, 12901 (2003); b) **G. Brannigan and F.L.H. Brown,** J. Chem. Phys., 122, 74905 (2005); c) **G. Illya, R. Lipowsky and J.C. Shillcock**, J. Chem. Phys., 122, 244901 (2005)

31 A**. Raudino** and **M. Pannuzzo** J. Chem. Phys, **132**, 045103 (2010)

32 **L.D. Landau, E.M. Lifsits**, Physical Kinetics, Pergamon Press, New York, 1985

33 (For a good review of early works see: **N. Duzgunes and D. Papahadjopoulos**, in: Membrane Fluidity in Biology, (R.C. Aloia ed.), Vol. 2, pp. 187-212, Academic Press, New York, 1983

34 **H. I. Petrache, N. Gouliaev, S. Tristam- Nagle, R. Zhang, R. M. Suter, and J. F. Nagle**, Phys. Rev. E **57**, 7014 (1998)

35 **S. Leikin, V. A. Parsegian, D. C. Rau, and R. P. Rand**, Annu. Rev. Phys. Chem. **44**, 369 (1993)

36 **T. J. McIntosh and S. A. Simon**, Biochemistry 32, 8374 (1993)

37 a) **B. R. Lentz, T. J. Carpenter, and D. R. Alford,** Biochemistry **26**, 5389 (1987) b) **B. R. Lentz, G. F. McIntyre, D. J. Parks, C. Yates, and D. Massenburg**, ibid. **31**, 2643 (1992) c) **D. Massenburg and B. R. Lentz**, ibid. **32**, 9172 (1993) d) **W. A. Talbot, L. X. Zeng, and B. R. Lentz**, ibid. 36, 5827 (1997)

38 **B. R. Lentz and J. K. Lee**, Mol. Membr Biol. **16**, 279 (1999)

39 a) **W. Helfrich**, Z. Naturforsch. C 33, 305 (1978) b) **J. N. Israelachvili and H. Wennerstrom**, J. Phys. Chem. **96**, 520 (1992) c) **R. R. Netz**, Phys. Rev. E **51**, 2286 (1995) d) **T. Gruhn and R. Lipowsky**, ibid. **71**, 011903 (2005)

40 (a) **E. Evans and D. Needham**, J. Phys. Chem., **91**, 4219 (1987) (b) **K.H. De Haas, C. Blom, D. Van den Ende, M.H.G. Duits and J. Mellema,** Phys. Rev. E, **56**, 7132 (1997)

(c) **T. Heimburg**, Biochim. Biophys. Acta, **1415**, 147 (1998) (d) **R.M. Hochmuth**, J. Biomech., **33**, 15 (2000) (e) **K. Mishima, S. Nakamae, H. Ohshima and T. Kondo**, Chem.Phys. Lipids, **110**, 27 (2001)

41 See, e.g., **G. Cevc and H. Richardsen**, Adv. Drug Delivery Rev. **38**, 207 (1999) and works cited therein

42 (a) **Y.A. Chizmadzhev, P.I. Kuzmin, A. Kumenko, J. Zimmerberg and F.S. Cohen**, Biophys. J **78**, 2241 (2000); (b) **P.I. Kuzmin, J. Zimmerberg, Y.A. Chizmadzhev and F.S. Cohen**, Proc. Natl. Acad. Sci. USA **98**, 7235 (2001); (c) **V.S. Markin and J.P. Albanesi**, Biophys. J. **82**, 693 (2002); (d) **Y. Kozlovsky, L.V. Chernomordik and M.M. Kozlov**, Biophys. J. **83**, 2634 (2002); (e) **Y. Kozlovsky and M.M. Kozlov**, Biophys. J. **82**, 882 (2002)

43 **P. G. DeGennes** Scaling Concepts in Polymer Physics, Cornell University Press, Ithaca N.Y (1979)

44 **H. Tang, K. F. Freed** J. Chem. Phys., **94**, 6307 (1991)

45 **I. Szleifer, B Widom** J. Chem. Phys., **90**, 7524 (1989)

46 See, e.g., Fuel Cells Research Trends, O. Vasquez ed., Nova Publ., New York, NY (2007)

47 **I. F. Hakem, J. Lal, M. R. Bockstaller,** Macromolecules **37**, 8431 (2004)

48 **R. A. Robinson, R. H. Stokes** Electrolyte Solutions, Butterworths, London (1959)

49 **U. Kaatze, 0. Gottmann, R. Podbielski, R. Pottel, U. Terveer**, J. Phys. Chem., **82**, 112 (1978)

50 **B. Y. Zaslawsky, L. M. Miheeva, M. N. Rodnikova, G. P. Spivak, V. S. Harkin, A. U. Mahmudov**, J Chem Soc Faraday Trans I, **85**, 2857 (1985)

51 **A. Vergara, L. Paduano L, R. Sartorio** Macromolecules, **35**, 1389 (2002)

52 **T. Shikata, R. Takahashi, A. Sakamoto**, J. Phys. Chem. B, **110**, 8941 (2006)

53 **L.D. Landau and E.M. Lifshitz,** Electrodynamics of Continuous Media. Pergamon Press, London (1980)

54 **P. Mallet, C.A. Guerin, A. Sentena,** Phys. Rev. B, **72**, 014205 (2005)

55 **L. Sandberg and O. Edholm**, J. Chem. Phys. **116**, 2936 (2002)

56 **M. J. Hey, D. P. Jackson and H. Yan**, Polymer **46**, 2567 (2005)

57 **P. Thiyagarajan, D. J. Chaiko, and R. P. Hjelm**, Macromolecules **28**, 7730 (1995)

58 **B.R. Lentz**, Chem Phys Lipids **73**, 91 (1994)

59 **R. Saez, A. Alonso, A.Villena, F.M. Goni**, FEBS Lett **137**, 323 (1982)

60 **L.T. Boni, T.P. Stewart, S.W. Hui**, J Membr Biol **80**, 91 (1984)

61 **K. Arnold, Y. Lvov, MSzogyi, S. Gyorgyi**, Stud Biophys **113**, 7 (1980)

62 **K. Arnold, A. Herrmann, K. Gawrisch, L. Pratsch**, Stud Biophys **110**, 135 (1985)

63 **K. Arnold, O. Zschoernig, D. Barthel, W. Herold W**. Biochim Biophys Acta **1022**, 303, (1990).

64 **E. Evans, D. Needham** , Macromolecules **21**,1822 (1998)

65 **T. Kuhl, Y.Q. Guo, J.L Alderfer, A.D. Berman, D.Leckband, J. Israelachvili, S.W. Hui**, Langmuir **12**, 3003 (1996)

66 **V.S. Malinin and B.R. Lentz**, Biochemistry **41**, 5913 (2002)

67 See, e.g., **D.F. Evans, H. Wennerstrom**, The Colloidal Domain, Wiley-VCH, New York, NY (1999)

68 **R. P. Rand and V. A. Parsegian**, Biochim. Biophys. Acta, **988**, 351 (1989)

69 **J. Formsnan, C.E. Woodward, B. Jonsson**, Langmuir, **23**, 5454 (1997)

70 **S. Asakura, and F. Oosawa**, J. Polym. Sci. **33**, 183 (1958)

71 **G. Cevc and D. Marsh**, Phospholipid Bilayers, Wiley, New York (1985)

72 **S. A. Tatulian**, in: Phospholipid Handbook, (G. Cevc ed.) Dekker, New York, 511 (1993)

73 **C.G. Sinn, M. Antonietti, R. Dimova**, Colloids and Surfaces A, **282**, 410 (2006)

74 **M. Arseneault, M. Lafleur**, Chem. Phys. Lipids **142**, 84 (2006)

75 Surfactants and Interface Phenomena, M.J. Rosen, Wiley, Hoboken, NJ (2004)

76 a) **M. Muller, K. Katsov, M. Schick**, J. Polym. Sci. B: Polym. Phys. **41**, 1441 (2003) b) **S.J. Marrink, A.H. de Vries, A.E. Mark**, J. Phys. Chem. B **108**, 750 (2004) c) **S.O. Nielsen, C.F. Lopez, G. Srinivas, M.L. Klei,** J. Phys.: Condens.Matter **16** R481, (2004)

77 a) **M. Muller, K. Katsov, M. Schick**, Phys. Rep., **434**, 113, (2006). b) **I. R. Cooke, M. Deserno**, J. Chem. Phys., **123** (2005). c) **I. R. Cooke, K. Kremer, M. Deserno**, Phys. Rev. E **72**, 011506, (2005) d) **G. Brannigan, L.C.L. Lin, F.L.H. Brown**, Eur. Biophys. J. **35**, 104, (2006)

78 a) **J. L. L. McWhirter, G. Ayton, G.A. Voth,** Biophys. J. **87**, 3242 (2004) b) **M. Neri,**

C. Anselmi, V. Carnevale, A.V. Vargiu, P. Carloni, J. Phys. Condens. Matter, **18**, S347 (2006) c) **M. Christen, W.F. van Gunsteren**, J. Chem. Phys. **124**, 154106 (2006) d) **M. Praprotnik, L.D. Site, K.J. Kremer**, Chem. Phys. **123**, 224106 (2005)

79 **S. J. Marrink, H. J. Risselada, S. Yefimov, D. P. Tieleman, and A. H. de Vries** J. Phys. Chem. B **111**,7812 (2007)

80 **H. J. Risselada, A. E. Mark and S.J. Marrink**, J. Phys. Chem. B **112**, 7438 (2008)

81 **S.O. Yesylevskyy, L.V.Shafer, D.Sengupta, S.J.Marrink,** PLoS Computational Biology **6**, 6 (2010)

82 **B. Hess, C. Kutzner, D. van der Spoel, & E. Lindahl,** J. Chem. Theory Comput **4,** 435 (2008)

83 **H. Lee, A. H. de Vries, S. J. Marrink, and R. W. Pastor** J Phys Chem B. **113**, 13186 (2009)

84 **H. J. C. Berendsen, J. P. M. Postma, W. F. van Gunsteren, A. DiNola, and J. R. Haak**. J. Chem. Phys. **81**, 3684 (1984)

85 **S. Forsen and J. Kordel**: Calcium in Biological Systems, in: Bioinorganic Chemistry, I. Bertini Ed., pp. 107-166, University Science Books, Michigan University, (1994)

86 **A. Raudino**, Theor. Chem. Acc., **111**, 141 (2004)

87 **O.A. Croze, M.A. Cates**, Langmuir, **2**, 5627 (2005)

88 **H. Huang, E. Ruckenstein**, Langmuir, **20**, 5412 (2004)

89 **D. Ben-Yaakov, D. Andelman, D. Harries, R. Podgornik**, J. Phys. Condens. Matter,

21, 424106 (2009)

90 **D. Ben-Yaakov, D. Andelman, D. Harries, R. Podgornik**, J. Phys. Chem. B, **113**, 6001 (2009)

91 **S. Buzzaccaro, R. Piazza, J. Colombo, A. Parola**, J. Chem. Phys,. **132,** 124902 (2010)

92 **A. Eliassi, H. Modarress, G. A. Mansoori,** J. Chem. Eng. Data, **44**, 52 (1999)

93 **K. Arnold, O. Zschoering, D. Barthel, W. Herold** Biochim. Biophys. Acta **1022**, 303 (1990)

94 **E. Evans, and D. Needham**. Macromolecules, **21**,1822 (1988)

95 **T.L. Kuhl, Y. Guo, J.L. Alderfer, A.D. Berman, D. Leckband, J.N. Israelachvili and S. W. Hui,** Langmuir, **12**, 3003 (1996)

96 **M. Ruths, H. Yoshizawa, L. J. Fetters, J. N. Israelachvili,** Macromolecules, **29**, 7193 (1996)

97 part I. **T. L. Kuhl, A. D. Berman, S. W. Hui, J. N. Israelachvili**, Macromolecules, **31**, 8250 (1998)

98 part II. **T. L. Kuhl, A. D. Berman, S. W. Hui, J. N. Israelachvili,** Macromolecules **31**, 8258 (1998)

99 **T. Bleha, P. Cifra**, Langmuir **20**, 764 (2004)

100 **H.L.S. Klapp, Y. Zeng, D. Qu, and R. von Klitzing,** Phys. Rev. Lett. **100**,118303 (2008)

101 **S. H. L. Klapp, S. Grandner, Y. Zeng and R. von Klitzing ,** Soft Matter**, 6**, 2330 (2010)

102 **M. Pelá ez-Fernández, A. Moncho-Jordá, J. Callejas-Fernández**, Europhys. Lett. 90, 46005 (2010)

103 **D. Rudhardt, C. Bechinger and P. Leiderer,** Phys. Rev. Lett. **81**, 1330 (1998)

104 **D. Rudhardt, C. Bechinger and P. Leiderer,** J. Phys.: Condens. Matter **11**, 10073 (1999)

105 **Y. N. Ohshima, H. Sakagami, K. Okumoto, A. Tokoyoda, T. Igarashi, K. B. Shintaku, S. Toride, H. Sekino, K. Kabuto and I. Nishio**, Phys. Rev. Lett. **78** 3963 (1997)

106 **G.W. Feigenson**, Biochemistry **25**, 5819 (1986)

107 **G.W. Feigenson**, Biochemistry **28**, 1270 (1989)

108 **A. Raudino, M. Pannuzzo**, J. Phys. Chem. B **114**, 15495 (2010)

109 **A. Vergara, L. Paduano, V. Vitagliano, R. Sartorio**, Macromolecules **34**, 9991-1000 (2001)

110 **K. Gawrisch, R. Thunich, U. Schulze, K. Arnold,** Mol. Cryst. Liq. Cryst. **152**, 333 (1987)

111 **L. A. Munishkina, E. M. Cooper, V. N. Uversky, A. L. Fink**, J. Mol. Recognit. **17**, 456 (2004)

112 **D. E. Leckband, C. A. Helm, and J. Israelachvili**, Biochemistry. **32**, 1127 (1993)

113 (a) **L. Chernomordik, M.M. Kozlov, J. Zimmerberg**, J. Membr. Biol**. 146**, 114 (1995)

(b) **R. Jahn, Grubmuller**, Curr. Opin. Cell Biol. **14**, 488 (2002) (c) **B. Lentz, V. Malinin, M.E. Haque, K. Evans**, Curr. Opin. Cell Biol. **10**, 607 (2000)

114 **G. Cevc**, Biochemistry **26**, 6305 (1987)

115 **G. Cevc, J. M. Seddon, D. Marsh**, Bioch. Et Biophys. Acta **814**, 141 (1985)

116 **S. W. Burgess, T. J. McIntosh, and B. R. Lentz**, Biochemistry **31**, 2653 (1992)

117 **V. S. Markin, M. M. Kozlov, and V. L. Borovjagin** Gen. Physiol. Biophys. **3**, 361 (1984)

118 **J. Heuvingh, F. Pincet and S. Cribier**, Eur. Phys. J. E **3**, 269 (2004)

119 **S. L. Leikin, M. M. Kozlov, L. V. Chernomordik, V. S. Markin, and Y. A. Chizmadzhev,** J. Theor. Biol **129**, 411(1987)

120 **F. Brochard and J.F. Lennon** J. Phys. France **36**, 1035 (1975)

121 **P. K. J. Kinnunen**, in Handbook of Nonmedical Application of Liposomes: Theory and Basic Sciences, D. D. Lasic and Y. Barenholz, Eds., pp. 153–171, CRC Press, 1996

122 **P. K. J. Kinnunen**, Chem. Phys. Lipids **81**, 151 (1996)

123 **T. D. Madden, P. R. Cullis**, Biochim. et Biophys. Acta **684**, 149, 1982

124 **R. P. Rand, N. L. Fuller, S. M. Gruner, and V. A. Parsegian**, Biochemistry **29**, 76 (1990)

125 **K. Lohner, G. Degovics, P. Laggner, E. Gnamusch, and F. Paltauf**, Biochim. et Biophys. Acta **1152**, 69 (1993)

126 **S. Nir, J. Wilschut, and J. Bentz**, Biochim. et Biophys. Acta **688**, 275 (1982)

127 **S.J. Marrink and A.E. Mark**, J. Am. Chem. Soc. **125**, 11144 (2003)

128 **D. Mirjanian, A.N. Dickey, J.H. Hoh, T.B. Woolf, M.J. Stevens**. J. Phys. Chem. B **114**, 11061 (2010)